

No Minima, No Collisions: Combining Modulation and Control Barrier Function Strategies for Feasible Dynamic Collision Avoidance

Yifan Xue[†] and Nadia Figueroa[†] *Member, IEEE*

Abstract—Control Barrier Function Quadratic Programs (CBF-QPs) have become a central tool for real-time safety-critical control due to their applicability to general control-affine systems and their ability to enforce constraints through optimization. Yet, they often generate trajectories with undesirable local minima that prevent convergence to goals. On the other hand, Modulation of Dynamical Systems (Mod-DS) methods (including normal, reference, and on-manifold variants) reshape nominal vector fields geometrically and achieve obstacle avoidance with few or even no local minima. However, Mod-DS provides no straightforward mechanism for handling input constraints and remains largely restricted to fully actuated systems. In this paper, we revisit the theoretical foundations of both approaches and show that, despite their seemingly different constructions, the normal Mod-DS is a special case of the CBF-QP, and the reference Mod-DS is linked to the CBF-QP through a single shared equation. These connections motivate our Modulated CBF-QP (MCBF-QP) framework, which introduces reference and on-manifold modulation variants that reduce or fully eliminate the spurious equilibria inherent to CBF-QPs for general control-affine systems operating in dynamic, cluttered environments. We validate the proposed controllers in simulated hospital settings and in real-world experiments on fully actuated Ridgeback robots and underactuated Fetch platforms. Across all evaluations, Modulated CBF-QPs consistently outperform standard CBF-QPs on every performance metric.

Index Terms—Concave obstacles, dynamical systems, control barrier functions, real-time motion and path planning, dynamic obstacles, collision avoidance, nonholonomic motion planning

I. INTRODUCTION

RECENT developments in autonomous systems have brought increasing research efforts into the field of robot obstacle avoidance and safe control system design. Autonomous robots colliding with environmental obstacles or their co-workers would not only reduce work efficiency but also injure users in safety-critical tasks ranging from autonomous driving to household human-robot interaction [1]. Thus, guaranteeing that a robot avoids unwanted collisions in our messy and dynamic world is necessary for safe deployment at scale. In the robotics literature, collision-free guarantees in dynamic environments are achieved through two algorithmic paradigms: either (i) via the satisfaction of constraints in **optimization-based** planners and safety filters, i.e., model predictive controllers (MPC) and control barrier functions (CBF) [2, 3, 4, 5, 6, 7], or (i) through **closed-form** potential-field inspired solutions that **geometrically warp** the navigation space, i.e., navigation functions, vector-field references and dynamical system (DS) modulation [8, 9, 10, 11, 12, 13, 14, 15]).

[†]Y. Xue and N. Figueroa are with the Department of Mechanical Engineering and Applied Mechanics, University of Pennsylvania, Philadelphia, PA 19104 USA {yifanxue, nadiafig}@seas.upenn.edu

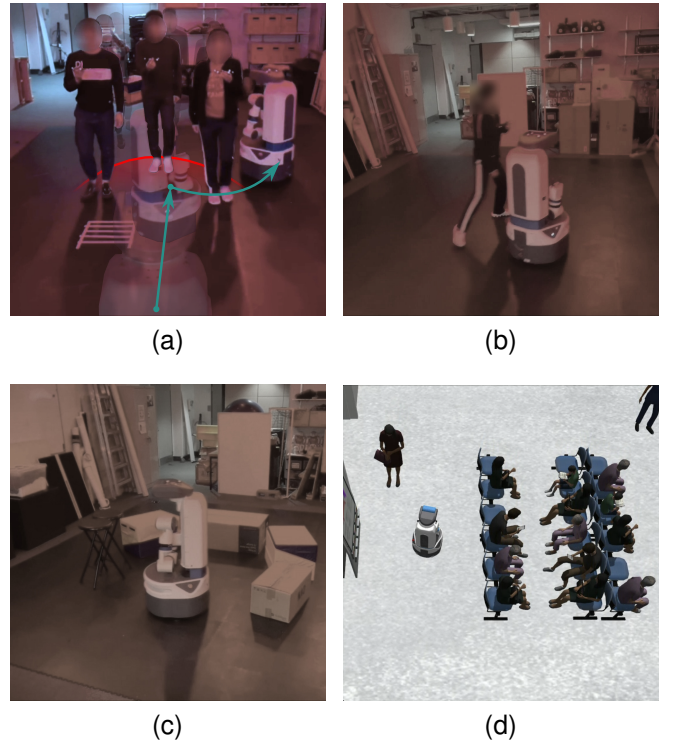


Fig. 1. Real-world experiments in (a) crowd navigation, (b) adversarial attack scenarios, and (c) concave obstacle navigation, together with a simulated experiment in (d) hospital navigation using Gazebo. All experiments are conducted using the proposed **MCBF-QP** strategy (Section VI) for local-minimum-free navigation in complex and dynamic environments.

In this paper, we study and compare the most competitive reactive control approaches representative of the current state-of-the-art in these two categories. For the first category, we examine Quadratic-Programming-based Control Barrier Functions (**CBF-QP**), which have gained considerable traction since the seminal work of Ames et al. [2]. For the second, we investigate Dynamical System Motion Policy Modulation (**Mod-DS**), originally introduced by Khansari and Billard [11]. Through this analysis, we demonstrate that although these techniques arise from distinct algorithmic paradigms, they are more similar than typically assumed. *Why is such a comparison necessary?* The motivation lies in the fact that both methods exhibit complementary strengths and limitations. A thorough theoretical, qualitative, and quantitative understanding of these characteristics motivates our proposed controller, the Modulated Control Barrier Functions (**MCBF-QP**) framework described in Section VI, which inherits the advantages of both approaches while mitigating their respective drawbacks.

CBF-QPs provide a generic framework for minimally adjusting a nominal controller while enforcing safety through affine inequality constraints derived from set invariance [2]. They offer several desirable properties, including applicability to general control-affine systems, smooth trajectory optimization, and explicit handling of actuation limits. Nevertheless, CBF-QPs are highly susceptible to local minima near even simple convex obstacles [16], and the issue exacerbates when multiple barrier functions interact in cluttered scenes. This vulnerability stems from the limited geometric structure encoded in the barrier functions. Prior work has shown that CBF-QPs, under some assumptions, are effectively equivalent to Artificial Potential Fields (APF) [8, 17], which are known to exhibit spurious equilibria requiring exploratory strategies to escape [18]. While this may appear to be a minor inconvenience, controllers that become trapped in configurations where progress toward the goal is halted (*despite a feasible path existing*) can severely disrupt task execution, degrade reliability, and induce unsafe or unpredictable behaviors in cluttered environments. In practice, such controllers may freeze, oscillate, or take unnecessarily conservative detours, which is unacceptable for robots operating around humans or in time-critical applications. Ensuring navigation strategies are **free of local minima** is therefore essential for guaranteeing consistent convergence to the goal, maintaining safety, and enabling reliable deployment in real-world, human-centric, dynamic settings.

Mod-DS approaches, inspired by Harmonic Potential Functions [10] and Navigation Functions [9], achieve obstacle avoidance by geometrically reshaping the robot’s motion vector field using a modulation matrix derived from the distances to, and gradient information of, nearby obstacles. The original Mod-DS formulation [11], which we refer to as the normal Mod-DS, was designed for convex obstacles and reduces the number of local minima compared to APFs. Yet it still exhibits spurious equilibria at obstacle boundaries when the nominal vector field becomes collinear with the obstacle gradient. This limitation was addressed in the reference Mod-DS [13], which introduces a gradient offset and leverages contraction theory to ensure that only a single spurious equilibrium (a saddle trajectory) exists for convex or star-shaped obstacles. More recently, [19] showed that this remaining equilibrium is unavoidable due to the Hairy Ball Theorem [20]. It instead proposed the on-manifold Mod-DS, which eliminates local minima entirely for arbitrary obstacle geometries by treating obstacle boundaries as navigable manifolds and constructing the modulation matrix from gradient, tangent, and curvature information. Although this latest formulation achieves local-minimum-free obstacle avoidance, all Mod-DS methods rely on closed-form geometric constructions that (i) are applicable to only fully actuated systems and (ii) cannot straightforwardly enforce actuation limits or general kinematic and dynamic constraints. This restricts their applicability to a narrow subset of robot morphologies, limiting deployment on real-world platforms with tight actuation budgets or underactuation.

Notably, the limitations of Mod-DS mirror the strengths of CBF-QPs, and vice versa. Therefore, when selecting a reactive safety controller, practitioners must currently choose between strong constraint handling and robustness to local

minima, as no existing method achieves both for general control-affine systems. In this paper, we present a novel approach that removes this trade-off. By analyzing and clarifying the behavioral similarities, differences, and theoretical connections between CBF-QP and Mod-DS methods, we introduce the **Modulated CBF-QP** control framework, which combines the strengths of both approaches while mitigating their respective drawbacks. The major contributions of this paper are as follows:

- 1) A theoretical and practical analysis, including equivalence results and a detailed comparison of Mod-DS and CBF-QP methods (Section IV, Section V).
- 2) A Modulated CBF-QP (MCFB-QP) control framework with two modulation variants that achieve local-minima reduction and, in particular, local-minimum-free obstacle avoidance for general control-affine systems (Section VI).
- 3) Extensive validation of the MCFB-QP controllers in simulation and on real robotic hardware (Section VII).

Similar works: Some prior comparisons have examined CLF-CBF QPs against Hamilton-Jacobi reachability methods in static environments [21], and others have contrasted optimization-based safe control with deep neural approaches. For example, [22] studies differences between deep learning and MPC for adaptive cruise control. However, a comprehensive comparison of reactive obstacle avoidance techniques in real-time dynamic settings remains absent. Although Mod-DS methods have gained traction for their computational efficiency and strong guarantees on reducing topologically unnecessary minima [13, 14, 19], they are rarely included in these evaluations. We believe our study fills this gap and provides substantial value to both the robotics research community and practitioners.

II. PROBLEM STATEMENT

Given the robot dynamics defined in Section II-A and the environment \mathcal{O} and controller assumptions stated in Section II-D, the objective is to design a control law $u(x, \mathcal{O})$ such that $\lim_{t \rightarrow \infty} x(t) = x^*$, while ensuring the resulting trajectories are free of collisions and undesirable local minima as defined in Section II-B and Section II-C.

A. Robot Dynamics

We restrict our study to *control-affine systems* defined as,

$$\dot{x} = f(x) + g(x)u, \quad (1)$$

where $x \in \mathbb{R}^d$, $u \in \mathbb{R}^p$, and f and g are Lipschitz continuous functions. A *fully actuated system*, as shown in Eq. (2), is a special case of a control-affine system where $p = d$:

$$\dot{x} = u. \quad (2)$$

B. Safety in Dynamic Obstacle Avoidance

Mod-DSs and CBF-QPs formalize robot safety and synthesize safe control algorithms using boundary functions. Given robot state $x \in \mathbb{R}^d$ and obstacle state $x_o \in \mathbb{R}^d$ for an obstacle o in the nearby obstacle set \mathcal{O} , a continuously \mathcal{C}^1 differentiable function $h_o : \mathbb{R}^d \times \mathbb{R}^d \rightarrow \mathbb{R}$ is a boundary function iff the safe set \mathcal{C}_o (outside the obstacle), the boundary set $\partial\mathcal{C}_o$ (on

the boundary of the obstacle), and the unsafe set $-\mathcal{C}_o$ (inside the obstacles) of the system can be defined as,

$$\begin{aligned} \mathcal{C}_o &= \{x \in \mathbb{R}^d, x_o \in \mathbb{R}^{d'} : h_o(x, x_o) > 0\} \\ \partial\mathcal{C}_o &= \{x \in \mathbb{R}^d, x_o \in \mathbb{R}^{d'} : h(x, x_o) = 0\} \\ -\mathcal{C}_o &= \{x \in \mathbb{R}^d, x_o \in \mathbb{R}^{d'} : h(x, x_o) < 0\} \end{aligned} \quad (3)$$

Note that the boundary function $h_o(x, x_o)$ can be simplified to $h_o(x)$ when the obstacle o is static (i.e., x_o is constant), and to $h(x, x_o)$ when the environment contains only a single obstacle. In practice, $h_o(x, x_o)$ is often represented as the distance from the controlled agent to the obstacle surface, i.e., the signed distance function. Given environments defined by h_o functions, the goal of a safety-critical controller is to generate an admissible input u that ensures the robot state x remains within the safe set \mathcal{C} , defined in Eq. (4), and ultimately reaches a target state $x^* \subset \mathcal{C}$.

$$\mathcal{C} = \{x \in \mathbb{R}^d, x_o \in \mathbb{R}^{d'} : h_o(x, x_o) > 0, \forall o \in \mathcal{O}\} \quad (4)$$

$$\partial\mathcal{C} = \{x \in \mathbb{R}^d, x_o \in \mathbb{R}^{d'} : h(x, x_o) = 0, \forall o \in \mathcal{O}\} \quad (5)$$

$$-\mathcal{C} = \{x \in \mathbb{R}^d, x_o \in \mathbb{R}^{d'} : h(x, x_o) < 0, \forall o \in \mathcal{O}\} \quad (6)$$

C. Local Minimum

Besides safety, a controller's navigation capability in complex environments also depends on how often it causes the robot to stop before reaching the intended target x^* . Following [13], we refer to such undesirable stops as *local minima*, also termed *critical points* in [23], *saddle equilibria* in [16] and *spurious attractors* in [14, 19].

Definition II.1 (Local Minimum in Robot Navigation). Let $\dot{x} = f(x, u)$ denote the robot dynamics, where $f : \mathbb{R}^d \times \mathbb{R}^p \rightarrow \mathbb{R}^d$. A point $x \in \mathbb{R}^d$ is called an *undesirable local minimum* if

$$f(x) = 0 \quad \text{and} \quad x \neq x^*,$$

i.e., the robot freezes at a point other than the target.

D. Assumptions

Controller: The safe controller takes as input the current robot state x , the nominal control u_{nom} , and outputs the desired safe action u to the system. When computing the action, we assume that the controllers have sufficient knowledge of the environment to accurately evaluate obstacle boundary functions $h_o(x, x_o), \forall o \in \mathcal{O}$.

Obstacles: In this work, we analyze and propose safe control methods capable of handling all obstacle geometries, including convex, star-shaped, and non-star-shaped concave obstacles. Star-shaped obstacles are defined as those containing a reference point from which every ray intersects the boundary exactly once [24]. Without loss of generality for applications in higher-dimensional state spaces, the methods are compared and validated in 2D navigation tasks. We define $p_{\text{rel}} = p - p_o \in \mathbb{R}^2$ as the relative position vector pointing from the obstacle o 's center p_o to the robot position p . Safe controllers' abilities in navigating around convex obstacles are tested using a circle with boundary function h_{conv} defined as,

$$h_{\text{conv}}(p_{\text{rel}}) = \|p_{\text{rel}}\|_2 - c_r, \quad (7)$$

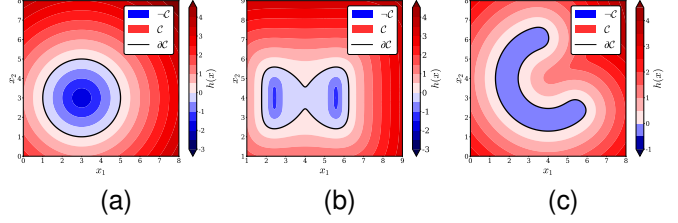


Fig. 2. Isolines displaying (a) h_{conv} , (b) h_{star} , and (c) h_{nstar} in the proximity of respectively a circle, a funnel, and a C-shaped obstacle.

where $c_r \in \mathbb{R}^+$ is the radius of the circle. Similarly, the ability of controllers to circumvent star-shaped obstacles is evaluated using a funnel-shaped obstacle with boundary function h_{star} defined in Eq. (8), where $C_a \in \mathbb{R}^2$ and $c_b \in \mathbb{R}^+$ are constants.

$$h_{\text{star}}(p_{\text{rel}}) = \|p_{\text{rel}} - C_a\|_4 - c_b \quad (8)$$

Finally, navigation around non-star-shaped concave obstacles is challenged with C-shape obstacles whose boundary function h_{nstar} is learned via the Gaussian Process Distance Field (GPDF) [25]. Isoline maps illustrating the change in h_{conv} , h_{star} , h_{nstar} values with respect to the relative positions of the robot are shown in Fig. 2. In this work, we focus on fixed-size obstacles that do not shrink, expand, or deform. All moving obstacles are assumed to exhibit only translational and rotational motion.

E. Notations

We use notation $\|\cdot\|_p$ to represent the p-norm of a vector and denote $\|\cdot\|_p^q = (\|\cdot\|_p)^q, \forall p, q \in \mathbb{Z}^+$. We annotate $\langle a, b \rangle$ for the dot product between vectors a and b . $\mathbf{0}_{a \times b}$ is a matrix full of 0s of size $a \times b$. Given a vector $a(\cdot)$, \hat{a} represents the axis whose direction is the same as $a(\cdot)$, and $a[:k]$ represents the new vector formed by the first k elements in a . Frequently-used variables in this work are summarized in Appendix A.

III. PRELIMINARIES

In this section, we review the CBF-QP and Mod-DS methods in single obstacle avoidance settings, denoting the boundary function $h_o(x, x_o)$ as $h(x, x_o)$.

A. Control Barrier Functions

In the CBF-QP formulation, the boundary function $h(x, x_o)$ is also known as the barrier function. To guarantee the safety of the controlled agent, CBF-QP utilizes the Nagumo Set Invariance Theorem.

Definition III.1 (Nagumo Set Invariance).

$$C \text{ is set invariant} \iff \dot{h}(x, x_o) \geq 0 \quad \forall x \in \partial\mathcal{C} \quad (9)$$

Control Barrier Functions extends Nagumo Set Invariance Theorem to a control setting [2], where the condition $\forall x \in \partial\mathcal{C}$ is rewritten mathematically using an extended \mathcal{K}_∞ function α .

$$\begin{aligned} C \text{ is set invariant} &\iff \\ \exists u \text{ s.t. } \dot{h}(x, x_o, \dot{x}_o, u) &\geq -\alpha(h(x, x_o)) \end{aligned} \quad (10)$$

TABLE I

PROPERTIES OF THE THREE MAIN MOD-DS VARIANTS, DETAILING THEIR DIAGONAL SCALING MATRIX $D(x, x_o)$, BASIS MATRIX $E(x, x_o)$, AND THE OBSTACLE TYPES THEY CAN TRAVERSE WITHOUT GENERATING TRAPPING REGIONS IN THE MODIFIED DS. THE TABLE ALSO LISTS THE NUMBER OF LOCAL MINIMA INDUCED PER OBSTACLE FOR THE NAVIGABLE OBSTACLE TYPES.

Property	$D(x, x_o)$	$d(x, x_o)$	Obstacle Type	# Minima
Normal [11]	$\lambda^*(x, x_o) = 1 - \frac{1}{h(x, x_o)+1}, \lambda_e^*(x, x_o) = 1 + \frac{1}{h(x, x_o)+1}$	$n(x, x_o)$	convex	1
Reference [13]	$\lambda^*(x, x_o) = 1 - \frac{1}{h(x, x_o)+1}, \lambda_e^*(x, x_o) = 1 + \frac{1}{h(x, x_o)+1}$	$r(x, x_o)$	convex, star-shaped	1
On-Manifold [19]	$D_\nabla(x, x_o) + D_\phi(x, x_o) + \varphi_h(x, x_o)D_h(x, x_o)$	$n(x, x_o)$	all \checkmark	0 \checkmark

Definition III.2 (Extended K_∞ Functions). An extended K_∞ function is a function $\alpha : \mathbb{R} \rightarrow \mathbb{R}$ that is strictly increasing with $\alpha(0) = 0$.

By enforcing the CBF conditions in Eq. (10) within a quadratic program, safety can be guaranteed through the set invariance of the safety region \mathcal{C} defined in Eq. (4). For general control affine systems, CBF-QP is formulated as follows,

$$u_{\text{cbf}} = \arg \min_{u \in \mathbb{R}^p} (u - u_{\text{nom}})^\top (u - u_{\text{nom}}) \quad (11)$$

$$L_f h(x, x_o) + L_g h(x, x_o)u + \nabla_{x_o} h(x, x_o)^\top \dot{x}_o \geq -\alpha(h(x, x_o))$$

For fully-actuated systems in Eq. (2), the CBF-QP becomes,

$$u_{\text{cbf}} = \arg \min_{u \in \mathbb{R}^d} (u - u_{\text{nom}})^\top (u - u_{\text{nom}}) \quad (12)$$

$$\nabla_x h(x, x_o)^\top u + \nabla_{x_o} h(x, x_o)^\top \dot{x}_o \geq -\alpha(h(x, x_o))$$

Closed-Form Solution: The CBF-QP admits closed-form solutions in single-obstacle environments when robot input limits are neglected. By solving the convex optimization problems in Eqs. (11) and (III-A) using the KKT conditions, the corresponding explicit CBF-QP solutions are given in Eqs. (13) and (14), respectively. For notational simplicity, we let $\alpha = \alpha(h(x, x_o)) + \nabla_{x_o} h(x, x_o)^\top \dot{x}_o$, $L_f h = L_f h(x, x_o)$, $L_g h = L_g h(x, x_o)$ and $\nabla_x h = \nabla_x h(x, x_o)$.

$$u_{\text{cbf}} = \begin{cases} u_{\text{nom}} & \text{if } L_f h + L_g h u_{\text{nom}} \geq -\alpha \\ u_{\text{nom}} - \frac{L_f h + L_g h u_{\text{nom}} + \alpha}{L_g h L_g h^\top} L_g h^\top & \text{otherwise} \end{cases} \quad (13)$$

$$u_{\text{cbf}} = \begin{cases} u_{\text{nom}} & \text{if } \nabla_x h^\top u_{\text{nom}} \geq \alpha \\ u_{\text{nom}} - \frac{\nabla_x h^\top u_{\text{nom}} + \alpha}{\nabla_x h^\top \nabla_x h} \nabla_x h & \text{otherwise} \end{cases} \quad (14)$$

B. Mod-DS Approach

Unlike CBF-QP that applies to general control-affine systems, Mod-DS is restricted to fully actuated systems. Mod-DS achieves obstacle avoidance by multiplying a full-rank locally active matrix $M(x, x_o) \in \mathbb{R}^{d \times d}$ with the nominal DS \dot{x}_{nom} , thereby reshaping the flow field. Specifically, it reduces the relative speed of the robot toward the obstacle while increasing or maintaining the speed along directions tangent to it [13, 14]. The smooth modulated DS \dot{x}_{mod} in the presence of an obstacle o , is computed as

$$\bar{\dot{x}}_o = \dot{x}_o^R + \omega_o \times (x - x_o^R), \quad (15)$$

$$u_{\text{mod}} = \dot{x}_{\text{mod}} = M(x, x_o)(\dot{x}_{\text{nom}} - \bar{\dot{x}}_o) + \bar{\dot{x}}_o, \quad (16)$$

where $x_o^R \in \mathbb{R}^d$ is the rotation center of obstacle o , and $\dot{x}_o^R, \omega_o \in \mathbb{R}^d$ are its linear and angular velocities, respectively. In a static scenario, Eq. (16) reduces to $\dot{x} = M(x)\dot{x}_{\text{nom}}$.

The modulation matrix $M(x, x_o)$ is constructed analogously to an eigendecomposition, with $E(x, x_o) \in \mathbb{R}^{d \times d}$ as the basis matrix and $D(x, x_o) \in \mathbb{R}^{d \times d}$ as the diagonal scaling matrix.

$$M(x, x_o) = E(x, x_o)D(x, x_o)E(x, x_o)^{-1} \quad (17)$$

$$D(x, x_o) = \text{diag}(\lambda(x, x_o), \lambda_e(x, x_o), \dots, \lambda_e(x, x_o)) \quad (18)$$

$$H(x, x_o) = [e_1(x, x_o) \ e_2(x, x_o) \ \dots \ e_{d-1}(x, x_o)] \quad (19)$$

$$E(x, x_o) = [d(x, x_o) \ H(x, x_o)] \quad (20)$$

The basis matrix $E(x, x_o)$, computed using Eq. (20), consists of a direction vector $d(x, x_o) \in \mathbb{R}^{d \times 1}$ pointing toward the obstacle and a hyperplane $H(x, x_o) \in \mathbb{R}^{d \times (d-1)}$ tangent to the obstacle surface, represented by an orthonormal basis $e_1(x, x_o), \dots, e_{d-1}(x, x_o) \in \mathbb{R}^{d \times 1}$ (see Eq. (19)). Velocity redistribution is enforced by the full basis matrix $E(x, x_o)$ along the directions $d(x, x_o), e_1(x, x_o), \dots, e_{d-1}(x, x_o)$, while the magnitudes along these directions are scaled by $D(x, x_o)$ as in Eq. (17). For multiple obstacles, a weighted sum of the individually stretched velocities is used [11]. There are three main variants of Mod-DS, differing in how $E(x, x_o)$ and $D(x, x_o)$ are constructed: normal, reference, and on-manifold Mod-DS [11, 13, 19], with their properties summarized in Table I. Since any smooth nondegenerate vector field, such as \dot{x}_{mod} , has at least as many topological local minima as obstacles [23], a variant is considered capable of handling a given obstacle type if its modified DS has at most one local minimum per such obstacle. All Mod-DS approaches ensure von Neumann impenetrability at the obstacle boundary [11, 13].

Normal Mod-DS [11]: In normal Mod-DS, the vector $n(x, x_o)$, normal to the surface of obstacle o and thus to the boundary function $h(x, x_o)$, is used as the direction toward the obstacle when constructing the basis matrix $E(x, x_o)$:

$$d_n(x, x_o) = n(x, x_o) = \frac{\nabla_x h(x, x_o)}{\|\nabla_x h(x, x_o)\|_2}. \quad (21)$$

Popular choices for the diagonal scaling matrix entries, $\lambda^*(x, x_o)$ and $\lambda_e^*(x, x_o)$, are listed in Table I, but any $\lambda(x, x_o)$ and $\lambda_e(x, x_o)$ satisfying

$$\lim_{h(x, x_o) \rightarrow 0} \lambda(x, x_o) = 0 \text{ and } \lambda_e(x, x_o) > 0, \ \forall x \in \mathbb{R}^d \quad (22)$$

are feasible. As the earliest proposed Mod-DS variant, normal Mod-DS guarantees convergence to the target x^* only in convex obstacle avoidance scenarios [11].

Reference Mod-DS [13]: Differs from normal Mod-DS

only in that it uses the reference direction $r(x, x_o)$ instead of $n(x, x_o)$ to form the basis matrix $E(x, x_o)$:

$$d_r(x, x_o) = r(x, x_o) = \frac{x - r^*(x_o)}{\|x - r^*(x_o)\|_2}. \quad (23)$$

Here, $r(x, x_o)$ points from the agent's current position x to the reference point $r^*(x_o) \in \mathbb{R}^d$ of obstacle o , as defined in [Definition III.3](#). This modification enables reference Mod-DS to handle star-shaped obstacles in addition to convex ones.

Definition III.3 (Reference Points in Star-Shaped Obstacles). A point $r^*(x_o) \in \mathbb{R}^d$ is a *reference point* if and only if it lies strictly inside the obstacle $-\mathcal{C}_o$ and every ray from $r^*(x_o)$ intersects the boundary $\partial\mathcal{C}_o$ exactly once. An obstacle or unsafe set is *star-shaped* if it contains at least one reference point.

On-Manifold Mod-DS [19]: Uses the same basis matrix $E(x, x_o)$ as the normal variant, i.e.,

$$d_{\text{onM}}(x, x_o) = n(x, x_o) = \frac{\nabla_x h(x, x_o)}{\|\nabla_x h(x, x_o)\|_2}. \quad (24)$$

However, unlike the other Mod-DS approaches that achieve safe control using a single uniform diagonal scaling policy as in Eq. (22), on-manifold Mod-DS realizes undesirable-equilibrium-free safe control through the combined effect of three navigation policies in the diagonal scaling matrix:

$$\lambda(x, x_o) = \lambda_\nabla(x, x_o) + \lambda_\phi(x, x_o) + \varphi_h(x, x_o)\lambda_h(x, x_o). \quad (25)$$

λ_∇ encodes the gradient descent dynamics, λ_ϕ enables on-manifold morphing dynamics, and λ_h defines the regular modulation dynamics. The technical details of on-manifold Mod-DS can be found in [19]. In this work, we focus on the obstacle exit strategy $\phi(x, x_o)$ used in λ_ϕ to efficiently circumnavigate both convex and concave unsafe regions. Let $e^{(0)}$ be one of m candidate directions in \mathbb{R}^{d-1} , with $e^{(0)} \notin \mathcal{N}(H(x, x_o))$ and $m \geq 2^{d-1}$. Geodesic approximation uses a first-order approximation of the obstacle surface to generate a path $X = [x^{(0)}, x^{(1)}, \dots, x^{(N)}]$ that exits the obstacle along its isosurface, where $N \in \mathbb{N}$ is the planning horizon [19]. the function $\phi(x, x_o) \in \mathbb{R}^d$ selects, among the m candidate directions, the one with the smallest associated potential P_N , which is computed iteratively using geodesic approximation as

$$\begin{aligned} x^{(i+1)} &= \beta H(x^{(i)}, x_o) H(x^{(i)}, x_o)^\top e^{(i)} + x^{(i)}, \\ e^{(i+1)} &= \frac{H(x^{(i)}, x_o) H(x^{(i)}, x_o)^\top e^{(i)}}{\|H(x^{(i)}, x_o) H(x^{(i)}, x_o)^\top e^{(i)}\|_2}, \\ P^{(i+1)} &= P^{(i)} + \beta p(x^{(i+1)}, x^*), \end{aligned} \quad (26)$$

β is the step size and $p(x, x^*)$ is a user-defined penalty function, typically chosen as the distance from x to the target x^* .

IV. CBF-QP AND MOD-DS PERFORMANCE COMPARISON ON DIFFERENT OBSTACLE GEOMETRIES

In this section, the Mod-DS variants specified in [Table I](#) and CBF-QP formulations with linear and exponential \mathcal{K}_∞ functions α are compared both qualitatively and quantitatively. All existing Mod-DS approaches are developed under the fully actuated system assumption; therefore, the conclusions

drawn here cannot be directly extended to general control-affine systems. For clarity of visualization in [Section IV-B](#) and for comparable quantitative metrics in [Section IV-C](#), we focus on single-obstacle avoidance in static environments. The insights gained from these comparisons form the foundation of the theoretical analysis presented in [Section V](#).

A. Nominal Dynamics & Obstacle Definition

We define the nominal controller u_{nom} to follow the integral curves of an autonomous linear 2D dynamical system (DS) as,

$$\dot{x}_{\text{nom}} = u_{\text{nom}} = -\epsilon x \quad \forall x \in \mathbb{R}^2, \quad (27)$$

with $\epsilon \in \mathbb{R}^+$. Three obstacle geometries are considered: i) a circle with $c_r = 2$ (Eq. (7)), ii) a star-shaped funnel with $C_a = [2.5, 0]^\top$ and $c_b = 0.1$ (Eq. (8)), and iii) an open ring with inner radius 2 and outer radius 2.3, as shown in [Fig. 2](#).

B. Qualitative Comparison

We begin by comparing qualitatively the performance of all methods in terms of obstacle geometry and trapping regions. [Fig. 3](#) presents stream plots of the safe DS \dot{x} resulting from CBF-QP and Mod-DS modifications, based on the nominal DS in Eq. (27). These plots demonstrate each method's effectiveness in preserving nominal dynamics while ensuring obstacle avoidance across various geometries.

Preservation of Nominal DS: In [Fig. 3](#), the streamline color indicates the relative speed magnitude of the modified controller compared to the nominal one, with yellow representing where the speed matches the nominal. Colors gradually fade toward blue or red as the modified speed becomes slower or faster than the nominal, respectively. Streamline curvature shows how the controller alters motion directions at each state. Qualitatively, CBF-QP generally preserves the nominal DS better than all Mod-DS variants, producing straighter streamlines more similar to the nominal linear DS (Eq. (27)) and larger yellow regions. Mod-DS approaches often increase speed along directions tangent to obstacles due to the λ_e parameter ([Table I](#)), and on-manifold Mod-DS can drastically alter or even reverse the nominal velocity directions because of the gradient descent dynamics in λ_ϕ . In addition, for CBF-QP, larger $\alpha(h)$ values lead to a larger feasible set for u , resulting in straighter streamlines and better preservation of the nominal DS.

Obstacle Geometries: While CBF-QPs and Mod-DSs differ in how well they preserve the nominal DS, they are similarly capable of avoiding convex obstacles. In these cases, trajectories exhibit no obvious trapping regions, except for a minor undesirable local minimum at the obstacle boundary where u_{nom} and $\nabla_x h(x, x_o)$ are collinear. A detailed analysis of this local minimum is provided in [Section IV-C](#). For concave obstacles, however, differences emerge. Plots 1(c)-5(c) and 1(e)-5(e) show CBF-QPs creating regions of attraction, where agents approaching opposite sides of the obstacle are guided toward a local minimum on the boundary. Normal Mod-DS exhibits similar trapping behavior. In contrast, reference Mod-DS avoids forming any region of attraction around star-shaped obstacles, and on-manifold Mod-DS remains free of those for all obstacle geometries. Therefore, reference and on-manifold

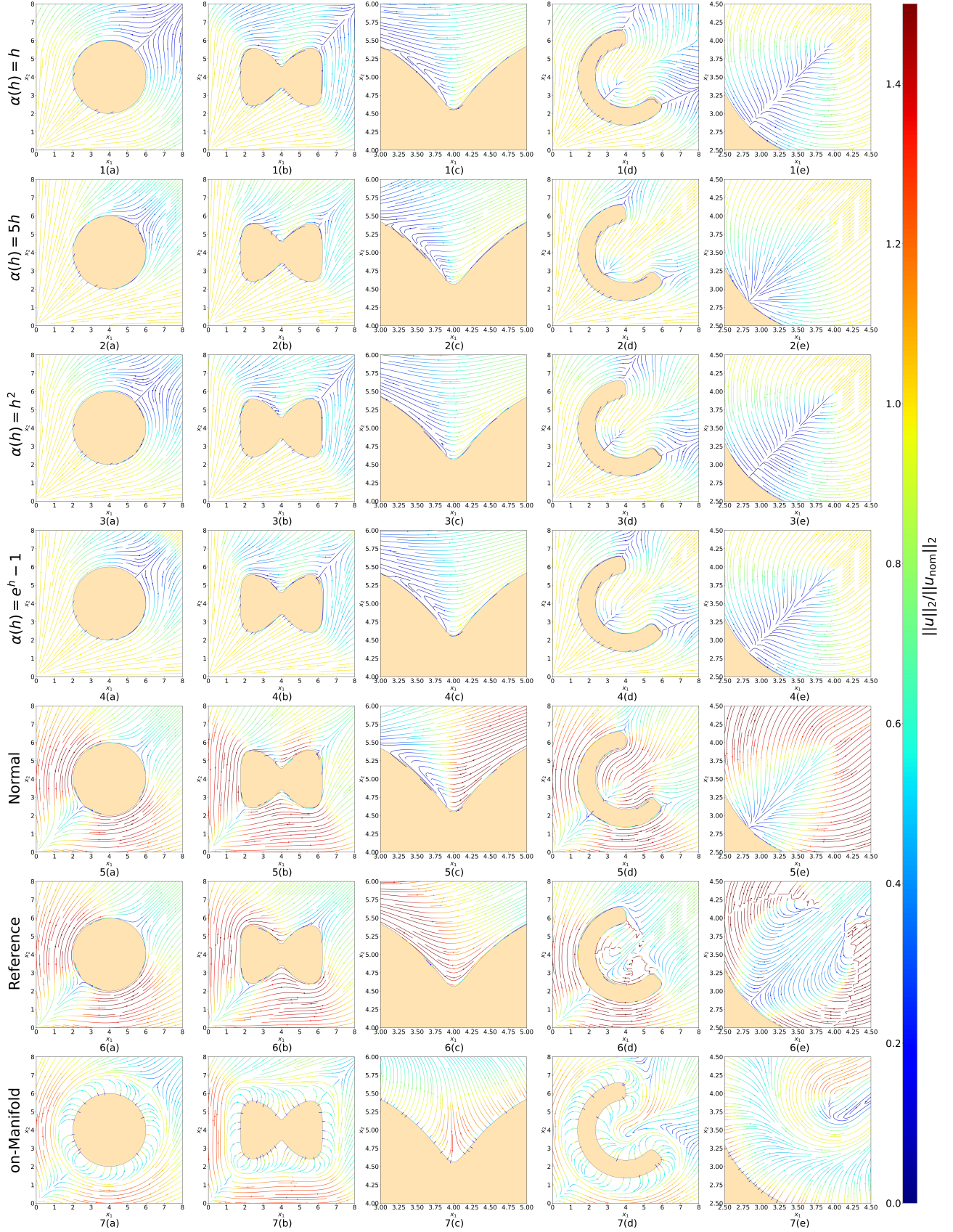


Fig. 3. Comparison of obstacle avoidance methods around convex, star-shaped, and non-star-shaped obstacles under the nominal linear DS in Eq. (27) with $\epsilon = 2$. Row 1-4 show CBF-QPs with different \mathcal{K}_∞ functions $\alpha(h)$, and the remaining rows show Mod-DS variants. Streamline colors represent the ratio of modified to nominal speeds, $\|u\|_2 / \|u_{\text{nom}}\|_2$.

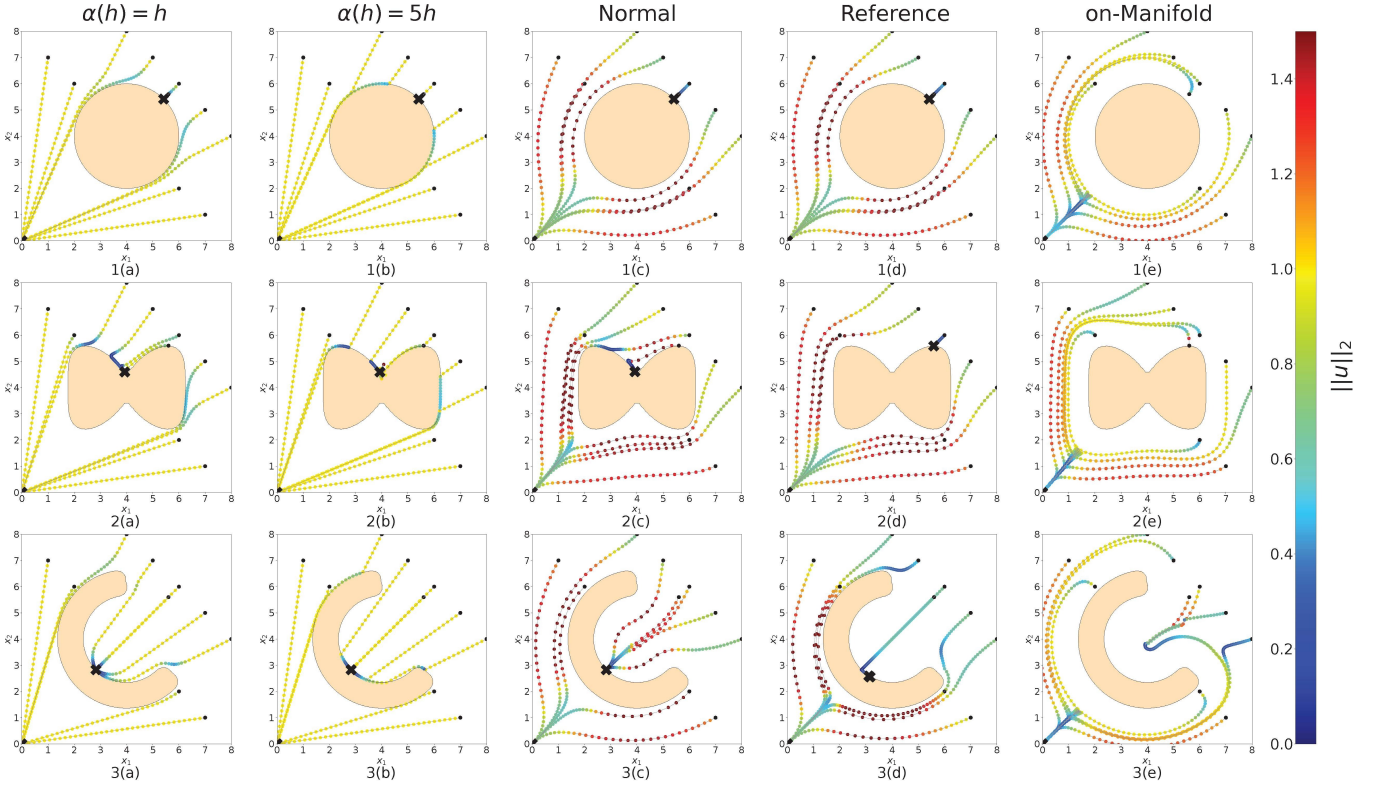


Fig. 4. Trajectories from 10 initial locations toward a target at the origin generated by CBF-QP (columns a-b) and Mod-DS (column c-e) obstacle avoidance methods around 1) a convex, 2) a star-shaped, and 3) a non-star-shaped obstacle. The nominal controller is $\epsilon = \frac{1}{\|x\|_2}$ (Eq. (27)). Colors along the trajectories indicate the robot speed magnitude at each state x .

Shape	Method	l/l_{nom} (std) ↓	\bar{j} (std) ↓	d_{obs} (std) ↑	v_{near} (std) ↓	η (std) ↓	Runtime [s] ↓	Success %
Convex	CBF-QP $\alpha = h$	1.03 (0.02)	1.32 (0.04)	2.43 (0.39)	0.96 (0.05)	0.34 (0.21)	0.0025	80
	CBF-QP $\alpha = 5h$	1.03 (0.03)	1.55 (0.03)	2.40 (0.41)	0.97 (0.04)	0.30 (0.22)	0.0026	80
	Normal Mod-DS	1.06 (0.03)	1.17 (0.04)	2.52 (0.41)	1.20 (0.02)	0.56 (0.07)	0.0002	80
	Reference Mod-DS	1.06 (0.03)	1.17 (0.04)	2.52 (0.41)	1.20 (0.02)	0.56 (0.07)	0.0002	80
	on-Mani Mod-DS	1.27 (0.17)	1.79 (0.71)	2.63 (0.34)	0.94 (0.10)	0.97 (0.13)	0.0004	100
Star	CBF-QP $\alpha = h$	1.03 (0.03)	1.55 (0.05)	2.39 (0.33)	0.95 (0.06)	0.49 (0.21)	0.0025	70
	CBF-QP $\alpha = 5h$	1.04 (0.04)	1.72 (0.06)	2.36 (0.35)	0.96 (0.06)	0.45 (0.21)	0.0025	70
	Normal Mod-DS	1.09 (0.07)	2.65 (0.68)	2.20 (0.40)	1.20 (0.07)	0.55 (0.07)	0.0002	90
	Reference Mod-DS	1.07 (0.05)	2.07 (0.68)	2.31 (0.37)	1.25 (0.04)	0.60 (0.04)	0.0002	80
	on-Mani Mod-DS	1.28 (0.17)	3.03 (1.16)	2.46 (0.26)	0.95 (0.12)	1.02 (0.09)	0.0005	100
C-shape	CBF-QP $\alpha = h$	1.02 (0.01)	1.31 (NA)	2.07 (0.24)	0.98 (0.03)	0.43 (NA)	0.0069	50
	CBF-QP $\alpha = 5h$	1.02 (0.02)	1.64 (NA)	2.06 (0.25)	0.99 (0.02)	0.39 (NA)	0.0057	50
	Normal Mod-DS	1.07 (0.03)	0.98 (NA)	2.13 (0.31)	1.30 (0.06)	0.64 (NA)	0.0065	50
	Reference Mod-DS	1.11 (0.06)	1.16 (0.08)	2.10 (0.28)	1.28 (0.06)	0.90 (0.25)	0.0055	80
	on-Mani Mod-DS	1.51 (0.34)	2.25 (0.44)	2.38 (0.15)	0.90 (0.10)	1.14 (0.04)	0.01224	100

TABLE II

CHARACTERISTICS OF TRAJECTORIES GENERATED BY MOD-DS AND CBF-QP APPROACHES FOR STATIC OBSTACLE AVOIDANCE AT A 5 HZ UPDATE FREQUENCY. METHODS PERFORMING WORST IN A METRIC ARE HIGHLIGHTED IN RED, AND THOSE PERFORMING BEST IN GREEN. METRICS COMPUTED FROM A SINGLE SUCCESSFUL TRAJECTORY HAVE THEIR STANDARD DEVIATIONS MARKED AS "NA".

Mod-DS offer more reliable navigation solutions in concave environments.

C. Quantitative Behavior Comparison

Quantitative analysis of the behavioral metrics for CBF-QP and Mod-DS is summarized in Table II. The evaluation uses the controller behavior metrics proposed in [26]: trajectory length l , average weighted jerk \bar{j} , straight-line deviation η , obstacle clearance d_{obs} , and near-obstacle velocity v_{near} . The straight-line deviation η quantifies how far the trajectory deviates from the nominal path, while the average weighted jerk \bar{j} reflects

trajectory smoothness and control feasibility. The obstacle clearance d_{obs} represents the mean distance between the robot and the nearest obstacle boundary along its trajectory, and the near-obstacle velocity v_{near} characterizes the robot's speed near obstacle boundaries. Metric formulations are provided in Appendix B. Ideal trajectories should exhibit small l/l_{nom} , low \bar{j} , high d_{obs} , low v_{near} , small η , short execution time, and high success rate. Each method in Table II was evaluated on 10 trajectories, with the resulting trajectories shown in Fig. 4. Note that behavior metrics l/l_{nom} , d_{obs} , and v_{near} were computed using only trajectories that successfully reached the

target. Metrics for \bar{j} and η were computed from the trajectories starting at $[4, 8]^\top$ and $[7, 5]^\top$ (if successful), as trajectories starting farther aside from the obstacles interact little with them and are less informative. Both Mod-DS and CBF-QP exhibit fast runtimes, suitable for dynamic environments. Mod-DS variants excel in adapting to diverse obstacle geometries via flexible eigenvector and eigenvalue choices. This enables on-manifold Mod-DS to avoid local minima entirely, achieving 100% target-reaching success and the highest obstacle clearance d_{obs} , though at the cost of slightly slower runtime, higher jerk \bar{j} , longer trajectories l , and larger straight-line deviation η . CBF-QP generates smooth, efficient trajectories with low \bar{j} , low v_{near} , and low length ratios l/l_{nom} , but suffers from lower target-reaching rates due to local minima. Normal Mod-DS performs similarly, but scaling factor $\lambda_e > 1$ increases tangent velocities, helping escape concave obstacle minima and yielding higher v_{near} and slightly better convergence. Reference Mod-DS matches normal Mod-DS in l/l_{nom} , d_{obs} , and v_{near} , while replacing the normal vector n with a reference vector r improves convergence for non-convex obstacles. Overall, reference and on-manifold Mod-DS are preferred over CBF-QP for concave obstacles in fully actuated systems, as CBF-QP's efficiency is offset by lower target-reaching rates.

V. THEORETICAL CONNECTIONS BETWEEN MOD-DS AND CBF-QP IN FULLY-ACTUATED SYSTEMS

The qualitative and quantitative analyses of Mod-DS and CBF-QP for fully actuated systems, in the prior section, revealed shared characteristics in static single-obstacle environments. Specifically, given the same input state x and nominal controller u_{nom} , both exhibit local minima caused by the collinearity between u_{nom} and $d(x)$, as will be shown analytically in Section V-A. Building on this observation, Section V-B demonstrates that normal Mod-DS is mathematically equivalent to CBF-QP under specific choices of λ and λ_e satisfying Eq. (22). Leveraging this equivalence, in Section VI-A we prove that reference Mod-DS satisfies the CBF conditions in Eq. (10) and derive a conversion relation with CBF-QP, revealing the closed-form structure that enables robust navigation in star-shaped obstacle environments with a single local minima. For clarity, we adopt the notations from the previous section and simplify the boundary function $h(x, x_o)$, direction vector $d(x, x_o)$, normal vector $n(x, x_o)$, and reference vector $r(x, x_o)$ to $h(x)$, $d(x)$, $n(x)$, and $r(x)$, respectively.

A. Local Minima in Mod-DS and CBF-QP

In normal and reference Mod-DS, the modified controllers fail to reach the target x^* whenever the nominal controller is inversely collinear with their directional vector $d(x)$, which is defined as the normal vector $n(x)$ for normal Mod-DS (Eq. (21)) and the reference vector $r(x)$ for reference Mod-DS (Eq. (23)).

Definition V.1 (Local Minima in Mod-DS). When the agent continuously encounters inverse collinearity between the directional vector $d(x)$ and nominal input u_{nom} , i.e., $\langle d(x), \frac{u_{\text{nom}}}{\|u_{\text{nom}}\|} \rangle = -1$, the resulting solutions of Eqs. (16)

and (17) drive the agent to an undesirable local minimum, $\dot{x} = u_{\text{mod}} \rightarrow \mathbf{0}$, on the obstacle boundary $\partial\mathcal{C}$ [11, 13].

Interestingly, few works have addressed undesirable local minima in CBF-QPs. Notomista et al. [27] identified this limitation but provided only a mitigation strategy without rigorous proof of their existence. In contrast, [16] analyzed CLF-CBF-QPs and showed that even convex obstacles can induce undesirable equilibria on boundaries due to conflicts between CLF and CBF constraints. Building on these insights, we formally prove that in fully actuated systems, undesirable local minima in CBF-QPs can also arise from inverse collinearity between the nominal controller and the normal vector $n(x)$, mirroring the mechanism observed in normal Mod-DS.

Theorem V.1 (Local Minima in CBF-QP). Consider a fully-actuated CBF-QP in a *static single-obstacle environment*. If a controller, starting at any initial state $x_{\text{ini}} \in \mathcal{C}$, **continuously** encounters inverse collinearity between $\nabla_x h(x)$ and u_{nom} , i.e., $\langle n(x), \frac{u_{\text{nom}}}{\|u_{\text{nom}}\|} \rangle = -1$, then the subsequent solutions of Eq. (III-A) (or equivalently Eq. (14)) will drive the agent to an undesirable local minimum, $\dot{x} = u_{\text{cbf}} \rightarrow \mathbf{0}$, at the obstacle boundary $\partial\mathcal{C}$.

Proof: Since $\nabla_x h(x)$ and u_{nom} are inversely collinear, there exists a constant scalar $c > 0$ such that $u_{\text{nom}} = -c\nabla_x h(x)$. Then Eq. (14) becomes

$$u_{\text{cbf}} = \begin{cases} -c\nabla_x h(x) & \text{if } \|\nabla_x h(x)\|_2^2 \leq -\frac{\alpha(h(x))}{c} \\ -\frac{\alpha(h(x))}{\|\nabla_x h(x)\|_2^2} \nabla_x h(x) & \text{otherwise} \end{cases}.$$

Case 1: If $\|\nabla_x h(x)\|_2^2 \leq -\frac{\alpha(h(x))}{c}$, then $u_{\text{cbf}} = -c\nabla_x h(x)$, and $\dot{h}(x) = \nabla_x h(x)^\top u_{\text{cbf}} = -c\|\nabla_x h(x)\|_2^2 < 0$. The robot moves toward the obstacle boundary until the inequality no longer holds, at which point the control switches to Case 2.

Case 2: If $\|\nabla_x h(x)\|_2^2 > -\frac{\alpha(h(x))}{c}$, then $u_{\text{cbf}} = -\frac{\alpha(h(x))}{\|\nabla_x h(x)\|_2^2} \nabla_x h(x)$. This continues to drive the robot along $-\nabla_x h(x)$, but the magnitude diminishes as $\alpha(h(x)) \rightarrow 0$ near the boundary.

In either case, the robot velocity vanishes at the obstacle boundary: $\lim_{h(x) \rightarrow 0} \dot{x} = \lim_{h(x) \rightarrow 0} u_{\text{cbf}} = \mathbf{0}$, so the robot gets trapped in an undesirable local minimum. ■

B. Normal Mod-DS and CBF-QP Equivalence

The similarity between normal Mod-DS and fully-actuated CBF-QP in terms of undesirable local minima originates from the fact that, in static environments, normal Mod-DS is equivalent to CBF-QP.

Theorem V.2 (Normal Mod-DS and CBF-QP Equivalence). In static environments, given fully-actuated CBF-QP controllers with any choice of extended K_∞ function α , there exists a pair of λ and λ_e such that normal Mod-DS defined in Eq. (16), (22) and (21) perform equivalently.

Proof: For simplicity, let $\alpha = \alpha(h(x))$, $\nabla_x h = \nabla_x h(x)$, $H = H(x)$, $E = E(x)$, and $M = M(x)$. Normal Mod-DS's basis matrix is $E = \begin{bmatrix} \nabla_x h \\ \|\nabla_x h\|_2 \end{bmatrix}$, according to Eqs. (20) and (21). Since $H^\top \nabla_x h = \mathbf{0}$ and the columns of H form an

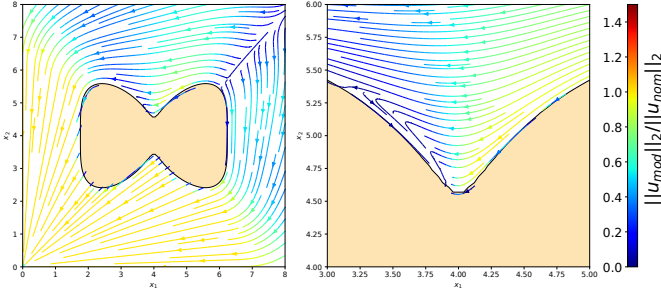


Fig. 5. Performance of the normal Mod-DS given λ , λ_e in Eq. (29) equivalent to that of CBF-QP with $\alpha(h) = h$ in Fig. 3.

orthonormal basis, E is an orthonormal matrix defining the *obstacle-based frame*. Therefore, $E^{-1} = E^\top$.

Projecting the CBF-QP solution into the obstacle-based frame defined by E gives

$$\begin{aligned} E^{-1}u_{\text{cbf}} &= E^\top u_{\text{cbf}} = \begin{bmatrix} \frac{\nabla_x h^\top}{\|\nabla_x h\|_2} \\ H^\top \end{bmatrix} u_{\text{cbf}} \\ &= \begin{cases} \begin{bmatrix} \frac{\nabla_x h^\top}{\|\nabla_x h\|_2} \\ H^\top \end{bmatrix} u_{\text{nom}} & \text{if } \nabla_x h^\top u_{\text{nom}} \geq -\alpha \\ \begin{bmatrix} \frac{\nabla_x h^\top}{\|\nabla_x h\|_2} \\ H^\top \end{bmatrix} u_{\text{nom}} - \begin{bmatrix} \frac{\nabla_x h^\top u_{\text{nom}} + \alpha}{\|\nabla_x h\|_2} \\ \mathbf{0}_{(d-1) \times d} \end{bmatrix} & \text{otherwise} \end{cases} \\ &= \begin{cases} \begin{bmatrix} \frac{\nabla_x h^\top}{\|\nabla_x h\|_2} \\ H^\top \end{bmatrix} u_{\text{nom}} & \text{if } \nabla_x h^\top u_{\text{nom}} \geq -\alpha \\ \begin{bmatrix} -\alpha \\ \frac{\|\nabla_x h\|_2}{} \\ H^\top u_{\text{nom}} \end{bmatrix} & \text{otherwise.} \end{cases} \end{aligned}$$

For the normal Mod-DS, projecting Eq. (16) with Eqs. (17), and (18) into the obstacle frame gives

$$\begin{aligned} E^{-1}u_{\text{mod}} &= E^{-1}Mu_{\text{nom}} = DE^\top u_{\text{nom}} \\ &= \begin{bmatrix} \lambda \frac{\nabla_x h^\top}{\|\nabla_x h\|_2} \\ \lambda_e H^\top \end{bmatrix} u_{\text{nom}}. \end{aligned} \quad (28)$$

Select λ and λ_e as shown in Eq. (29). Since $\alpha = \alpha(h) \rightarrow 0$ as $h \rightarrow 0$ by the property of K_∞ functions, λ and λ_e trivially satisfy the requirements in Eq. (22).

$$\lambda = \begin{cases} 1 & \text{if } \nabla_x h^\top u_{\text{nom}} \geq -\alpha \\ -\frac{\alpha}{\nabla_x h^\top u_{\text{nom}}} & \text{otherwise} \end{cases} \quad \text{and } \lambda_e = 1. \quad (29)$$

Substituting Eq. (29) into (28) yields

$$\begin{aligned} E^{-1}u_{\text{mod}} &= \begin{cases} \begin{bmatrix} \frac{\nabla_x h^\top}{\|\nabla_x h\|_2} \\ H^\top \end{bmatrix} u_{\text{nom}} & \text{if } \nabla_x h^\top u_{\text{nom}} \geq -\alpha \\ \begin{bmatrix} -\alpha \\ \frac{\|\nabla_x h\|_2}{} \\ H^\top u_{\text{nom}} \end{bmatrix} & \text{otherwise} \end{cases} \\ &= E^{-1}u_{\text{cbf}}. \end{aligned}$$

Because two vectors that are identical in one coordinate system are identical in all coordinate systems, we conclude that $u_{\text{cbf}} = u_{\text{mod}}$ when λ and λ_e are chosen as in Eq. (29). ■

To further validate Theorem V.2, we compute normal Mod-DS's λ and λ_e from Eq. (29) given $\alpha(h) = h$, and plot the

resulting modified DS in Fig. 5. The directions and magnitudes (color-coded) of the streamlines produced by this normal Mod-DS exactly match those of the corresponding CBF-QP modified DS shown in Fig. 3 1(b) and 1(c).

C. Reference Mod-DS and CBF-QP Similarities

In Section IV-B, the performance of the reference Mod-DS was demonstrated to be superior to that of the CBF-QP. Nevertheless, the fact that reference Mod-DS shared the same undesirable local minimum with CBF-QPs for circular obstacle avoidance in Fig. 4 suggests the potential for hidden connections between the two seemingly distinctive approaches. Quantifying the similarities and differences between reference Mod-DS and CBF-QP is key to understanding how undesirable local minima can be reduced or even eliminated to realize global convergence. We begin our discussion here by proving u_{mod} from reference Mod-DS satisfies the CBF constraints at all times in static-single-obstacle avoidance and then quantify what changes need to be introduced before reference Mod-DS and CBF-QP can be unified. The theoretical connections discussed here will contribute to the design of a new safe control approach that incorporates the advantage of reference Mod-DS and CBF-QP in Section VI.

Theorem V.3 (Safe Set Invariance in Reference Mod-DS). Given fully-actuated nominal controller u_{nom} in Eq. (2) and any λ and λ_e satisfying Eq. (22), there exists an extended class K_∞ function such that the Mod-DS safe controller u_{mod} defined in Eq. (16), (17), and (23) meets the CBF conditions defined in Eq. (III-A) when $\dot{x}_o = \mathbf{0}$.

In static-single obstacle avoidance scenarios, annotations can be simplified such that $h = h(x, x_o)$ and $\nabla_x h = \nabla_x h(x, x_o)$. Given $\dot{x}_o = \mathbf{0}$ and $\ddot{x}_o = \mathbf{0}_{d \times 1}$, CBF conditions in Eq. (III-A) can be rewritten as:

$$\frac{\nabla_x h^\top}{\|\nabla_x h\|_2} u \geq -\frac{\alpha(h)}{\|\nabla_x h\|_2}. \quad (30)$$

Following the same notation as in Theorem V.2, $\forall x \in \mathbb{R}^d$, denote $r = r(x, x_o)$, $n = n(x, x_o)$, $e_i = e_i(x, x_o)$, $\forall i \in \{1, 2, \dots, d-1\}$ and $H = [e_1(x, x_o), \dots, e_{d-1}(x, x_o)] \in \mathbb{R}^{d \times (d-1)}$ to be the hyperplane plane orthogonal to the gradient of the boundary function $\nabla_x h$. Let the basis matrix of reference Mod-DS $E_r = [r(x, x_o), H(x, x_o)] \in \mathbb{R}^{d \times d}$, as defined in Eq. (20) and (23). Note that $\|r(x, x_o)\|_2 = 1$ by definition. Since $E_r(x, x_o)$ is not an orthonormal basis, $E_r^{-1} \neq E_r^\top$. Instead,

$$\begin{aligned} E_r^{-1} &= \begin{bmatrix} \frac{1}{\nabla_x h^\top r} \nabla_x h^\top \\ -\frac{1}{\nabla_x h^\top r} e_1^\top r \nabla_x h^\top + e_1^\top \\ \vdots \\ -\frac{1}{\nabla_x h^\top r} e_{d-1}^\top r \nabla_x h^\top + e_{d-1}^\top \end{bmatrix} \\ &= \begin{bmatrix} \frac{1}{\nabla_x h^\top r} \nabla_x h^\top \\ H^\top (I - \frac{1}{\nabla_x h^\top r} r \nabla_x h^\top) \end{bmatrix}. \end{aligned} \quad (31)$$

Therefore, the decomposition of u_{mod} onto r by basis matrix E_r when $\dot{x}_o = 0$ can be computed from Eq. (16), (17) as

$$u_{\text{mod}}^r = \lambda E_r^{-1} [1, :] u_{\text{nom}} = \frac{\nabla_x h^\top}{\nabla_x h^\top r} \lambda u_{\text{nom}}.$$

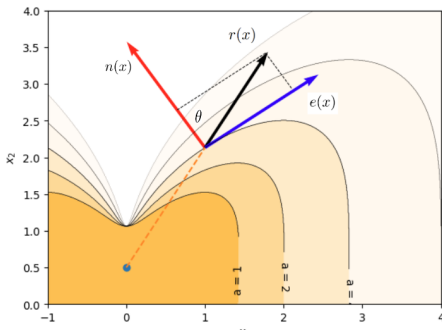


Fig. 6. Illustration of the geometric interpretation and relationship between $n(x)$, $e(x)$ and $r(x)$ used for [Theorem V.3](#).

The decomposition of u_{mod} onto r can be further broken down into the direction n parallel to $\nabla_x h$ and into the tangent hyperplane H orthogonal to $\nabla_x h$, as depicted in [Fig. 6](#). The projection of u_{mod}^r onto n is equivalent to u_{mod}^n , the projection of u_{mod} onto n , because the vector H is orthogonal to n , i.e. $n^\top H = \mathbf{0}_{1 \times d-1}$.

$$\begin{aligned} u_{\text{mod}}^n &= n^\top (u_{\text{mod}}^r r + u_{\text{mod}}^H e) = u_{\text{mod}}^r n^\top r \\ &= \left(\frac{\nabla_x h^\top}{\|\nabla_x h^\top\|} \lambda u_{\text{nom}} \right) \left(\frac{\nabla_x h}{\|\nabla_x h\|_2} \right)^\top r \\ &= \lambda u_{\text{nom}} \frac{\nabla_x h^\top}{\|\nabla_x h\|_2} \end{aligned} \quad (32)$$

Now we are left with showing the modulated value in [Eq. \(32\)](#) satisfies the CBF conditions. *WTS*: Given any $\nabla_x h, h, u_{\text{nom}}$ and λ combinations, there exists a K_∞ function α such that the following inequality, acquired by substituting $\frac{\nabla_x h^\top}{\|\nabla_x h\|_2} u = u_{\text{mod}}^n$ and u_{mod}^n expression from [Eq. \(32\)](#) into [Eq. \(30\)](#) and simplify, always holds.

$$-\lambda \nabla_x h^\top u_{\text{nom}} \leq \alpha(h)$$

Since the norms of $\nabla_x h, u_{\text{nom}}$ and λ values are all well-bounded by definition, find α that serve as an upper bound for domain $\{x \in \mathbb{R}^d : h(x, x_o) > 0\}$ is trivial. When $h(x, x_o) = 0$, $\lambda = 0$ based on [Eq. \(22\)](#), the left and right sides of the inequality become 0 and satisfy the property of K_∞ functions. In conclusion, given a bounded fully-actuated nominal controller u_{nom} in [Eq. \(2\)](#) and any feasible λ and λ_e , there exists an extended class K_∞ function such that the Mod-DS safety controller u_{mod} meets the CBF conditions. ■

Theorem V.4 (Quantitative Difference between Reference Mod-DS and CBF-QP). Given any CBF-QP with a fully-actuated nominal controller u_{nom} in [Eq. \(2\)](#), there exist a pair of λ, λ_e values satisfying [Eq. \(22\)](#) such that the differences between outputs from reference Mod-DS and CBF-QP can be quantified as $(\lambda_e - \lambda) \sum_{i=1}^{d-1} \frac{e_i^\top r}{n^\top r} e_i n^\top u_{\text{nom}}$. In the expression, we abuse notation and let $r = r(x, x_o)$ in [Eq. \(23\)](#), $e_i = e_i(x, x_o)$ [Eq. \(19\)](#) and $n = n(x, x_o)$ in [Eq. \(21\)](#).

Proof: Since both normal and reference Mod-DS are reactive safe control approaches with explicit closed-form solutions, given the same λ and λ_e , the differences between reference and normal Mod-DS in regions where both are active can be computed as in [\[19\]](#). Here to distinguish reference Mod-DS outputs from the normal ones, we denote results from reference

Mod-DS as u_{mod}^R and that from the normal one as u_{mod}^N .

$$u_{\text{mod}}^R = u_{\text{mod}}^N - (\lambda_e - \lambda) \sum_{i=1}^{d-1} \frac{e_i^\top r}{n^\top r} e_i n^\top u_{\text{nom}}$$

Because CBF-QP is demonstrated to be equivalent to normal Mod-DS in [Theorem V.2](#), setting reference Mod-DS to be only active in scenarios where CBF-QP is, i.e. $u_{\text{mod}}^R = u_{\text{nom}}$ when $\nabla_x h^\top u_{\text{nom}} \geq -\alpha$ similar to [Eq. \(14\)](#), it can be trivially concluded that,

$$\begin{aligned} &u_{\text{mod}}^R - u_{\text{cbf}} \\ &= \begin{cases} \mathbf{0} & \text{if } \nabla_x h^\top u_{\text{nom}} \geq 0 \\ -(\lambda_e - \lambda) \sum_{i=1}^{d-1} \frac{e_i^\top r}{n^\top r} e_i n^\top u_{\text{nom}} & \text{otherwise} \end{cases} \end{aligned} \quad (33)$$

Given the theoretical connections between normal and reference Mod-DS to CBF-QP derived in this section we propose a novel CBF-QP formulation augmented by either reference or on-manifold modulation-style constraints. ■

VI. MODULATED CONTROL BARRIER FUNCTIONS (MCBF)

Mod-DS approaches excel in fully actuated systems, navigating non-convex unsafe sets with far fewer undesirable local minima than CBF-QP. Yet, CBF-QP remains prevalent in robotics due to its applicability to general control-affine systems and guaranteed actuation compliance. Ideally, users **should not have to face a tradeoff** between effectively handling complex dynamics and avoiding local minima in obstacle navigation. To bridge this gap, we propose the Modulated CBF-QP (**MCBF-QP**) control framework with two variants: (i) reference modulated, described in [Section VI-A](#), applicable for efficient star-shaped obstacle avoidance and (ii) on-manifold modulated, described in [Section VI-B](#), for navigating arbitrary concave obstacle environments.

A. Reference MCBF for Star-shaped Obstacle Avoidance

In [Theorem V.3](#), reference Mod-DS and CBF-QP are shown to perform similarly along the $n(x, x_o)$ direction. [Theorem V.4](#) highlights that the introduction of off-diagonal components in the tangent hyperplane $H(x, x_o)$ is the main theoretical difference between CBF-QP and reference Mod-DS in fully actuated systems, and the key factor in reducing undesirable local minima during star-shaped obstacle avoidance. This insight suggests that adding constraints on u_{cbf} along the tangent hyperplane can mitigate local minima caused by standard CBF constraints. Practically, there are numerous ways to incorporate the off-diagonal components into CBF-QP results. Below, we propose a **linear constraint formulation**, referred to as Reference MCBF-QP (R-MCBF-QP), that is mathematically simple and preserves the computational efficiency of the original CBF-QP problem.

$$\begin{aligned} &u_{\text{mcbf}} = \arg \min_{u \in \mathbb{R}^p, \rho \in \mathbb{R}^{d-1}} (u - u_{\text{nom}})^\top (u - u_{\text{nom}}) + \rho^\top \rho \quad (34) \\ &L_f h(x, x_o) + L_g h(x, x_o) u + \nabla_{x_o} h(x, x_o)^\top \dot{x}_o \geq -\alpha(h(x, x_o)) \\ &H(x, x_o)^\top \left(I - \frac{r(x, x_o) \nabla_x h(x, x_o)^\top}{\nabla_x h(x, x_o)^\top r(x, x_o)} \right) g(x) (u - u_{\text{nom}}) = \rho \end{aligned}$$

Note that the following term:

$$E_r(x, x_o)^{-1}[2 : d, :] \dot{x} = H(x, x_o)^\top \left(I - \frac{r(x, x_o) \nabla_x h(x, x_o)^\top}{\nabla_x h(x, x_o)^\top r(x, x_o)} \right) \dot{x}$$

represents the projection of \dot{x} onto the hyperplane $H(x, x_o)$ in the non-orthogonal basis $E_r(x, x_o)$, ρ is the relaxation parameter. The terms $g(x)$ and $E_r(x, x_o)^{-1}$ are defined in Eqs. (1) and (31), respectively.

For fully-actuated systems in Eq. (2), R-MCBF-QP can be simplified to,

$$u_{\text{mcbf}} = \arg \min_{u \in \mathbb{R}^d, \rho \in \mathbb{R}^{d-1}} (u - u_{\text{nom}})^\top (u - u_{\text{nom}}) + \rho^\top \rho \quad (35)$$

$$\nabla_x h(x, x_o)^\top u + \nabla_{x_o} h(x, x_o)^\top \dot{x}_o \geq -\alpha(h(x, x_o))$$

$$H(x, x_o)^\top \left(I - \frac{r(x, x_o) \nabla_x h(x, x_o)^\top}{\nabla_x h(x, x_o)^\top r(x, x_o)} \right) (u - u_{\text{nom}}) = \rho.$$

In summary, the affine constraints highlighted in blue in Eqs. (34) and (35) project velocities onto the hyperplane, mirroring the reference Mod-DS approach and effectively reducing local minima in CBF-QP. They ensure that safe control outputs avoid undesirable equilibria, except when \dot{x}_{nom} is inversely collinear with the reference direction $r(x, x_o)$. The added constraints are designed to be of linear equality types and thus would not cause large runtime increases. Additionally, the introduction of the relaxation parameter ρ sustains the feasibility of the regular CBF-QP. In other words, given the same x and x_o , R-MCBF-QP will be feasible if and only if the CBF-QP without our additional constraints is feasible. The performance of fully-actuated R-MCBF-QP in star-shaped obstacle environments, using the fully actuated system defined in Eq. (2) and the linear nominal controller u_{nom} from Eq. (27), is validated in Fig. 7.

Explicit Solutions of Reference MCBF-QP: When there is only one unsafe set in the environment and robot actuation limits are ignored, explicit solutions can be derived for R-MCBF-QP, as with standard CBF-QP. To theoretically demonstrate R-MCBF-QP's ability to reduce undesirable equilibria, we derive its explicit solution from the fully actuated problem formulation in Eq. (35) and analyze it through the lens of Theorem V.4.

Derivation: Following the assumptions and notations in Theorem V.4, we again consider static-single-obstacle scenarios with $\dot{x}_o = \mathbf{0}$ and define $\alpha = \alpha(h(x, x_o))$, $H = H(x, x_o)$, $r = r(x, x_o)$, and $\nabla_x h = \nabla_x h(x, x_o)$. The R-MCBF-QP in Eq. (35) can be reformulated into the following Lagrangian function, where $\mu_{\text{eq}} \in \mathbb{R}^{d-1}$ and $\mu_{\text{cbf}} \in \mathbb{R}$ are the Lagrange multipliers.

$$\begin{aligned} L(u, \rho, \mu_{\text{eq}}, \mu_{\text{cbf}}) &= (u - u_{\text{nom}})^\top (u - u_{\text{nom}}) + \rho^\top \rho \\ &+ \mu_{\text{eq}}^\top \left[\rho - H^\top \left(I - \frac{r \nabla_x h^\top}{\nabla_x h^\top r} \right) (u - u_{\text{nom}}) \right] \\ &- \mu_{\text{cbf}} (\nabla_x h^\top u + \alpha) \end{aligned}$$

According to the Karush–Kuhn–Tucker theorem, the necessary (and here sufficient) conditions for u_{mcbf} and ρ^* to solve the R-MCBF-QP are:

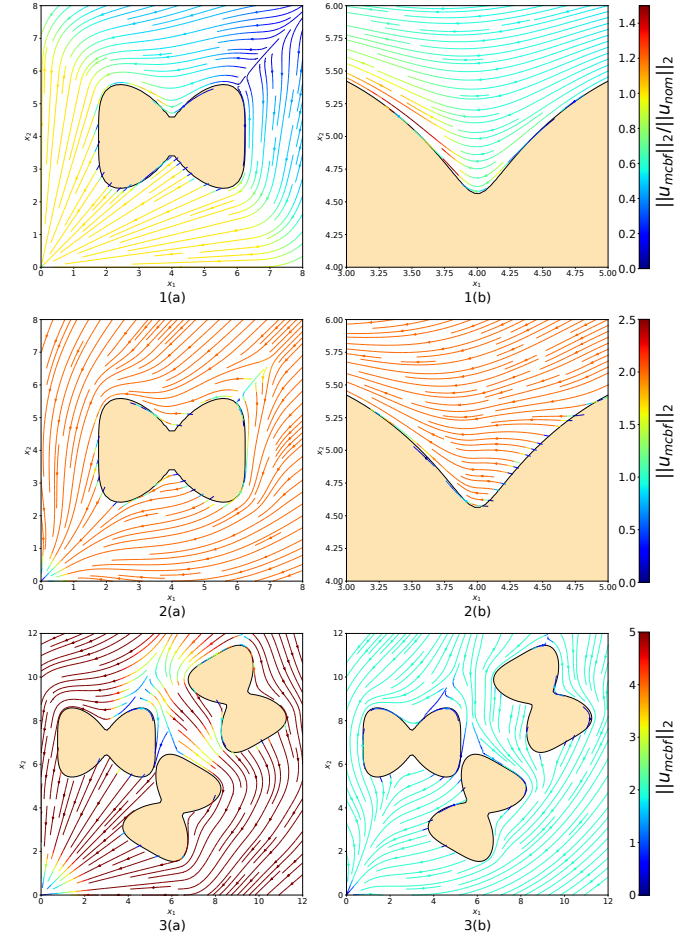


Fig. 7. Performance of reference MCBF-QP in single obstacle avoidance with no robot input constraints (first row, (a): full view, (b): close view), in single obstacle avoidance with robot input constraints of $\|u_{\text{mcbf}}\|_2 \leq 2$ (second row, (a): full view, (b): close view), and in multi-obstacle avoidance respectively with and without robot input constraints of $\|u_{\text{mcbf}}\|_2 \leq 2$ (third row (a) and (b)).

Stationarity: $\nabla_{u_{\text{mcbf}}, \rho} L(u_{\text{mcbf}}, \rho^*, \mu_{\text{eq}}, \mu_{\text{cbf}}) = 0$

Inequality: $\nabla_x h^\top u_{\text{mcbf}} + \alpha \geq 0$

Equality: $H^\top \left(I - \frac{r \nabla_x h^\top}{\nabla_x h^\top r} \right) (u_{\text{mcbf}} - u_{\text{nom}}) = \rho^*$

Dual: $\mu_{\text{cbf}} \geq 0$

Slackness: $\mu_{\text{cbf}} (\nabla_x h^\top u_{\text{mcbf}} + \alpha) = 0$

Solving these conditions yields the explicit solution

$$u_{\text{mcbf}} = \begin{cases} u_{\text{nom}} & \text{if } \nabla_x h^\top u_{\text{nom}} + \alpha \geq 0 \\ F^{-1}(I + \nabla_x h A) F u_{\text{nom}} + A^\top \alpha & \text{otherwise} \end{cases}, \quad (36)$$

where

$$F = 2 \left[I + \left(I - \frac{r \nabla_x h^\top}{\nabla_x h^\top r} \right)^\top \left(I - \frac{r \nabla_x h^\top}{\nabla_x h^\top r} \right) \right], \quad (37)$$

and

$$A = -\frac{\nabla_x h^\top F^{-1}}{\nabla_x h^\top F^{-1} \nabla_x h}. \quad (38)$$

From Fig. 6, observe that the vector $r(x, x_o)$ can be written as a weighted sum of the unit normal direction $n(x, x_o)$ and the orthonormal basis vectors $\{e_i(x, x_o)\}_{i=1}^{d-1}$ spanning the

hyperplane H . This gives the representation

$$r = w_0 n + \sum_{i=1}^{d-1} w_i e_i \quad \text{and} \quad \sum_{i=0}^{d-1} (w_i)^2 = 1 \quad (39)$$

with coefficients $w_i \in \mathbb{R}^+$. $\sum_{i=0}^{d-1} (w_i)^2 = 1$ follows from the fact that $r(x, x_o)$ is a unit vector by definition. For brevity, we again write $n = n(x, x_o)$ and $e_i = e_i(x, x_o)$. From Eq. (21), we know that $\nabla_x h = \|\nabla_x h\|_2 n$. Substituting the above decompositions of r and $\nabla_x h$ into Eq. (37) reveals that F is orthogonally diagonalizable with respect to the basis $E = [n \ H]$, introduced in Eqs. (20) and (21).

$$F = E \Lambda E^\top,$$

where

$$\Lambda = \begin{bmatrix} \frac{2}{(w_0)^2} & -\frac{2}{w_0} W^\top \\ -\frac{2}{w_0} W & 4I_{d-1} \end{bmatrix} \quad \text{and} \quad W = \begin{bmatrix} w_1 \\ \vdots \\ w_{d-1} \end{bmatrix}.$$

Since E is an orthogonal matrix, its inverse equals its transpose:

$$F^{-1} = (E \Lambda E^\top)^{-1} = E \Lambda^{-1} E^\top. \quad (40)$$

Applying the Schur complement inversion formula to the block-partitioned matrix Λ produces

$$\Lambda^{-1} = \begin{bmatrix} k & \frac{k}{2w_0} W^\top \\ \frac{k}{2w_0} W & \frac{1}{4} I_{d-1} + \frac{k}{4(w_0)^2} W W^\top \end{bmatrix}, \quad (41)$$

where

$$k = \left(\frac{2}{(w_0)^2} - \frac{1}{(w_0)^2} W^\top W \right)^{-1} = \frac{(w_0)^2}{1 + (w_0)^2}$$

because $W^\top W = \sum_{i=1}^{d-1} (w_i)^2 = 1 - (w_0)^2$, according to Eq. (39). Substituting Eqs. (40), (41) into Eq. (38) yields the compact expression

$$A = \frac{1}{2\|\nabla_x h\|_2} (n^\top + \frac{1}{w_0} r^\top).$$

In conclusion, the explicit solution of R-MCBF-QP u_{mcbf} can be equivalently expressed in terms of the normal vector n and reference vector r as,

$$\begin{cases} u_{\text{nom}} & \text{if } \nabla_x h^\top u_{\text{nom}} + \alpha \geq 0 \\ u_{\text{nom}} - \frac{1}{2w_0} (w_0 n n^\top + r n^\top) u_{\text{nom}} + \alpha A^\top & \text{otherwise} \end{cases} \quad (42)$$

Remark: The explicit solution of regular CBF-QP in fully-actuated systems, defined using Eq. (14), can be rewritten using n as

$$u_{\text{cbf}} = \begin{cases} u_{\text{nom}} & \text{if } \nabla_x h^\top u_{\text{nom}} + \alpha \geq 0 \\ u_{\text{nom}} - (n n^\top u_{\text{nom}} + \frac{\alpha}{\|\nabla_x h\|_2} n) & \text{otherwise} \end{cases} \quad (43)$$

Given u_{mcbf} derived in Eq. (42), the difference between the two explicit solutions is

$$u_{\text{mcbf}} - u_{\text{cbf}} = \begin{cases} \mathbf{0} & \text{if } \nabla_x h^\top u_{\text{nom}} + \alpha \geq 0 \\ -\frac{1}{2w_0} (r - w_0 n) n^\top u_{\text{nom}} + \alpha (A^\top + \frac{n}{\|\nabla_x h\|_2}) & \text{otherwise} \end{cases}$$

On the boundary of the unsafe sets, i.e., when $\alpha = 0$, this reduces to

$$u_{\text{mcbf}} - u_{\text{cbf}} = \begin{cases} \mathbf{0} & \text{if } \nabla_x h^\top u_{\text{nom}} \geq 0 \\ -\frac{1}{2w_0} (r - w_0 n) n^\top u_{\text{nom}} & \text{otherwise} \end{cases} \quad (44)$$

From Eq. (39), we know that $n^\top r = w_0$ and $e_i^\top r = w_i$ for $i \in \{1, 2, \dots, d-1\}$. Therefore, when $\alpha = 0$, the quantitative relationship between reference Mod-DS and regular CBF-QP, deduced in Eq. (33), can be reformulated as

$$u_{\text{mod}}^r - u_{\text{cbf}} = \begin{cases} \mathbf{0} & \text{if } \nabla_x h^\top u_{\text{nom}} \geq 0 \\ -\frac{\lambda_e - \lambda}{w_0} (r - w_0 n) n^\top u_{\text{nom}} & \text{otherwise} \end{cases} \quad (45)$$

Observe that when $\lambda_e - \lambda = \frac{1}{2}$, the differences $u_{\text{mcbf}} - u_{\text{cbf}}$ in Eq. (44) and $u_{\text{mod}}^r - u_{\text{cbf}}$ in Eq. (45) are identical for arbitrary u_{nom} and $\nabla_x h$. Since λ and λ_e can take any real values satisfying Eq. (22), there exist infinitely many (λ, λ_e) pairs that fulfill $\lambda_e - \lambda = \frac{1}{2}$. Hence, there always exist feasible (λ, λ_e) pairs such that outputs of the reference MCBF-QP match those of reference Mod-DS on boundaries of the unsafe sets. This guarantees that reference MCBF-QP is free of undesirable equilibria except when u_{nom} is inversely collinear to $r(x, x_o)$ in the boundary set $\partial\mathcal{C}$.

B. On-Manifold MCBF for Non-star-shaped Obstacle Avoidance

By retaining the standard CBF-QP constraints to capture Mod-DS policies along the normal direction $n(x, x_o)$, and introducing new constraints in Eqs. (34) and (35) to emulate the reference Mod-DS actions within the tangent hyperplane $H(x, x_o)$, the proposed reference MCBF-QP effectively integrates the advantages of both approaches, enabling QP-based star-shaped obstacle avoidance. While on-manifold Modulation, functioning under the aggregate effects of three policies, is too structurally complicated to be explicitly connected to CBF-QP on a theoretical level, it similarly regulates \dot{x} along $n(x, x_o)$ and avoids undesirable local minima by ordering tangent-space motions via $\phi(x, x_o)$. Motivated by this insight, we incorporate $\phi(x, x_o)$ -induced $H(x, x_o)$ constraints into CBF-QP, yielding the on-manifold MCBF-QP variant (onM-MCBF-QP). For general control-affine systems, local-minimum-free safe navigation for arbitrary obstacle shapes can be achieved via the following optimization problem:

$$u_{\text{mcbf}} = \arg \min_{u \in \mathbb{R}^p} (u - u_{\text{nom}})^\top (u - u_{\text{nom}}) \quad (46)$$

$$L_f h(x, x_o) + L_g h(x, x_o) u + \nabla_{x_o} h(x, x_o)^\top \dot{x}_o \geq -\alpha (h(x, x_o)) \\ \phi(x, x_o)^\top f(x) + \phi(x, x_o)^\top g(x) u \geq \gamma.$$

The parameter γ is a user-defined positive real number, i.e. $\gamma \in \mathbb{R}^+$. Unlike reference MCBF-QP, which remains feasible whenever the original CBF-QP without the additional $H(x, x_o)$ constraint is feasible, the feasible domain of on-manifold MCBF-QP is always smaller due to the proposed tangent hyperplane inequality constraint. Additionally, the larger γ is, the smaller the feasible domain of on-manifold MCBF-QP will be.

For fully-actuated systems, as in Eq. (2), the special case of CBF-QP can be simplified as to:

$$\begin{aligned} u_{\text{mcbf}} &= \arg \min_{u \in \mathbb{R}^d, \rho \in \mathbb{R}^{d-1}} (u - u_{\text{nom}})^\top (u - u_{\text{nom}}) \quad (47) \\ \nabla_x h(x, x_o)^\top u + \nabla_{x_o} h(x, x_o)^\top \dot{x}_o &\geq -\alpha(h(x, x_o)) \\ \phi(x, x_o)^\top u &\geq \gamma. \end{aligned}$$

In both Eq. (46) and (47), the additional $H(x, x_o)$ constraint highlighted in blue projects the system's velocity onto the tangent hyperplane via the exit strategy $\phi(x, x_o)$, analogous to the on-manifold Mod-DS approach [19] described in Section III-B. Further implementation details on how the geodesic approximation method can be extended from its traditional Euclidean-space application to non-Euclidean robot state spaces are provided in Section VII-B. The performance of on-manifold MCBF-QP in concave obstacle environments, using the fully actuated system defined in Eq. (2) and the linear nominal controller u_{nom} from Eq. (27), is validated in Fig. 8.

Remark: While reference MCBF-QP can, in theory, be extended to nonlinear dynamical systems as in Eq. (34), its application to high-dimensional systems is limited because determining reference directions $r(x, x_o)$ becomes nontrivial when $d > 3$, and the computational complexity increases with d . However, given a proper step size β , the geodesic approximation method in Eq. (26) is able to closely approximate unsafe set boundaries for any given state $x \in \mathbb{R}^d$. As a result, on-manifold MCBF-QP can be readily applied in any control affine robot system given a reasonably designed barrier function $h(x, x_o)$.

VII. ROBOT EXPERIMENT

The obstacle avoidance performance of the proposed MCBF-QP controllers (Section VI) is validated in Gazebo simulations using the omnidirectional-drive Ridgeback and differential-drive Fetch robots, against Mod-DS and CBF-QP baselines. Since the original Mod-DS approaches in [11, 13, 19] do not account for robot actuation limits, we instead perform simulations with our modified speed-constraining Mod-DS documented in Appendix D. This variant we proposed optimally enforces robot speed constraints while maintaining theoretical safety guarantees. To assess the effectiveness of the proposed onM-MCBF-QP in real-world underactuated robot navigation, the algorithm was deployed on a hardware Fetch robot and compared with that of the standard CBF-QP. Throughout all simulations and hardware experiments, the proposed MCBF controllers and the baseline methods are tasked with traveling from their initial position to the target while avoiding collisions with obstacles along the path, with control inputs updated at 20 Hz. The robots are assumed to be able to detect all obstacles within a 3-meter sensing range.

A. Robot Dynamics

For fully actuated systems, the trajectories generated by the proposed reference and on-manifold MCBF-QP methods (R-MCBF-QP and onM-MCBF-QP) are compared with those from the CBF-QP and constrained Mod-DS baselines through physics-based Gazebo experiments using an omnidirectional

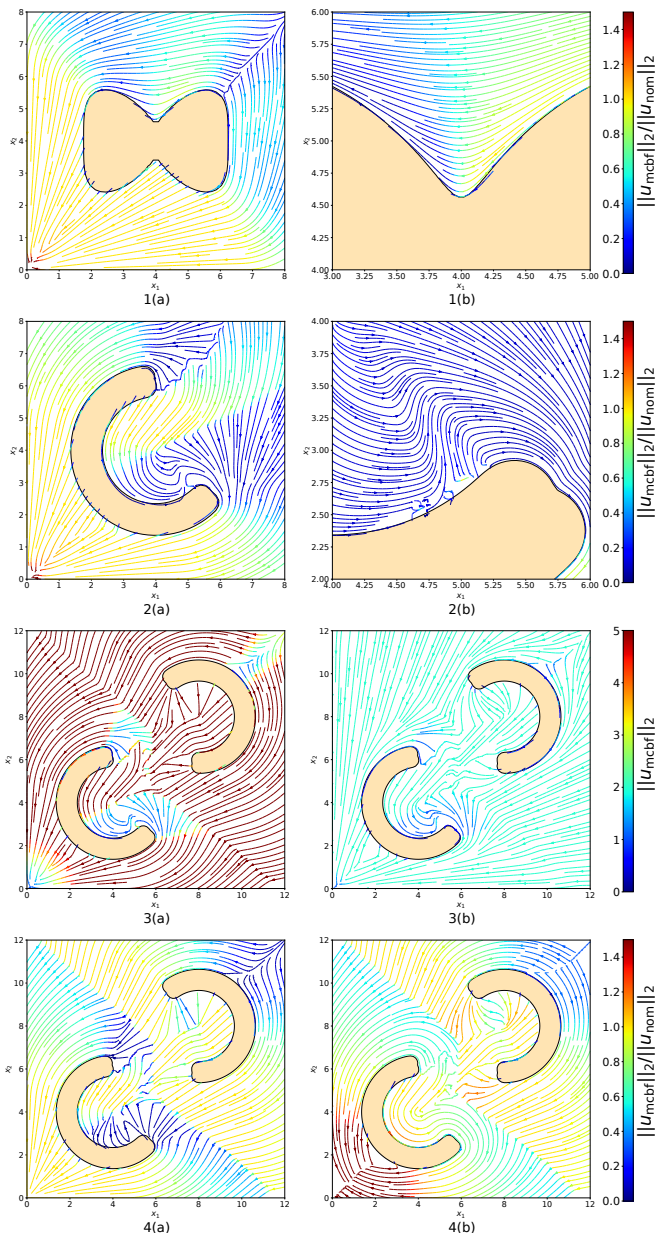


Fig. 8. Performance of on-manifold MCBF-QP in single star-shaped (first row) and non-star-shaped (second row, (a): full view, (b): close view) obstacle avoidance with no robot input constraints, in multi-concave obstacle avoidance (third row, (a): without input constraints, (b): with robot input constraints of $\|u_{\text{mcbf}}\|_2 \leq 2$), given $\gamma = 1$. Lastly, pictures on the fourth row show the effects of γ sizes on the resulted safe trajectories ((a): $\gamma = 0.1$, (b): $\gamma = 10$).

Ridgeback robot. The Ridgeback is modeled as a holonomic platform with first-order kinematics:

$$\begin{bmatrix} \dot{p}_x \\ \dot{p}_y \end{bmatrix} = \begin{bmatrix} u_x \\ u_y \end{bmatrix}, \quad (48)$$

where p_x and p_y denote the robot's position along the x - and y -axes, respectively.

For underactuated systems, controller performance is evaluated using a differential-drive Fetch robot in Gazebo. Each controller computes control inputs based on the standard

unicycle kinematic model:

$$\dot{x} = \begin{bmatrix} \dot{p}_x \\ \dot{p}_y \\ \dot{\theta} \end{bmatrix} = \begin{bmatrix} \cos \theta & 0 \\ \sin \theta & 0 \\ 0 & 1 \end{bmatrix} \begin{bmatrix} v \\ \omega \end{bmatrix}, \quad (49)$$

where v and ω denote the linear and angular velocities, respectively.

Because the barrier functions $h(x, x_o)$ defined in Section II-D depend only on position, their partial derivatives with respect to the orientation are zero, i.e., $\partial h / \partial \theta = 0$. As a result, the CBF constraint in Eq. (11) simplifies to

$$\frac{\partial h}{\partial p_x} \dot{p}_x + \frac{\partial h}{\partial p_y} \dot{p}_y + \nabla_{x_o} h \dot{x}_o \geq -\alpha(h).$$

Substituting \dot{p}_x and \dot{p}_y from Eq. (49) into the above expression shows that the resulting CBF-QP depends only on v , while ω does not appear. Consequently, the standard CBF-QP cannot directly regulate the robot's heading, which often limits its ability to guarantee obstacle avoidance.

1) *Shifted-Model Approach*: To address this limitation, we shift the robot's reference point by a distance $a > 0$ along its heading, yielding the modified kinematic model

$$\dot{x} = \begin{bmatrix} \dot{p}_x \\ \dot{p}_y \\ \dot{\theta} \end{bmatrix} = \begin{bmatrix} \cos \theta & -a \sin \theta \\ \sin \theta & a \cos \theta \\ 0 & 1 \end{bmatrix} \begin{bmatrix} v \\ \omega \end{bmatrix}. \quad (50)$$

This shift couples the translational and rotational dynamics, allowing both v and ω to directly affect the barrier function. Hence, the MCBF-QP and CBF-QP controllers can jointly regulate translation and heading for safe navigation. A practical advantage of this formulation is that on-manifold MCBF-QP can compute the guiding vector $\phi(x, x_o)$ used in Eq. (46) through simple geodesic approximation in the two-dimensional Euclidean position space, similar to the fully actuated case. However, this trick is robot-specific and not readily generalizable to other underactuated robots. We therefore develop a more general on-manifold MCBF-QP implementation that performs geodesic approximation in the non-Euclidean configuration space $[p_x, p_y, \theta]^T$. For clarity, controllers using the shifted model are denoted S-onM-MCBF-QP and S-CBF-QP, and those using the augmented CBF as A-onM-MCBF-QP and A-CBF-QP.

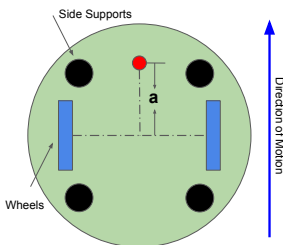


Fig. 9. Reference point shift along the robot's heading in the shifted unicycle model.

2) *Augmented-CBF Approach*: To handle general underactuated systems, we design an augmented control barrier

function that incorporates the robot's orientation into the barrier definition:

$$h_{\text{aug}}(x, x_o) = h(p_x, p_y, x_o) + w \frac{\partial h}{\partial p_x} \cos \theta + w \frac{\partial h}{\partial p_y} \sin \theta, \quad (51)$$

where $w \in \mathbb{R}^+$ is a design parameter. The added terms capture how the robot's heading aligns with the gradient of the barrier function, introducing explicit dependence on θ . This orientation embedding allows the controller to account for rotational effects directly through the barrier function, without altering the kinematic model. Substituting h_{aug} for h in the classical CBF constraint yields the augmented CBF constraints used in the A-CBF-QP and A-onM-MCBF-QP formulations.

Nominal Controller: For fully actuated systems, the nominal controller u_{nom}^l in Eq. (27) with $\epsilon = 1/\|x\|_2$ is used on the Ridgeback platform. For underactuated systems, the nominal control inputs are approximated from the linear dynamical system as

$$v_{\text{nom}} = \|u_{\text{nom}}^l\|_2, \quad \omega_{\text{nom}} = \frac{\psi}{\Delta t}, \quad (52)$$

where ψ is the angular difference between the current orientation θ and the desired orientation inferred from u_{nom}^l , and Δt is the control update period. This approximation is inexact due to the nonholonomic constraints of differential-drive robots.

B. Geodesic Approximation in Non-Euclidean Space

In [19], the geodesic approximation-based obstacle exit strategy, given appropriately tuned step size β and horizon N , generates a first-order approximation of a locally optimal path circumventing an obstacle in Euclidean space \mathbb{R}^d . Crucially, this path identifies $\phi(x, x_o)$, the tangent direction along the obstacle surface that the robot should follow to efficiently navigate around the obstacle. In this work, we show that the geodesic approximation equations in Eq. (26) can similarly provide tangent-hyperplane guidance in non-Euclidean robot state spaces x . This enables Modulated CBF-QP, particularly its $\phi(x, x_o)$ constraint, to be theoretically applied to general control-affine systems.

In the experimental section, we validate the application of this strategy in a 3-dimensional non-Euclidean state space using the unicycle model $x = [p_x, p_y, \theta]^T$. Fig. 10 (a)–(c) illustrate the unsafe region defined by the augmented CBF in Eq. (51) within our constructed 3D non-Euclidean state space. For clarity and interpretability, only the section with $\theta \in [0, 2\pi)$ is shown. Starting from the robot state $x^{(0)} = [3, 3, 0]$, we generate 20 vectors $e^{(0)}$ evenly distributed in the plane tangent to the gradient of $h_{\text{aug}}(x^{(0)}, x_o)$. Using the geodesic approximation strategy, the tangent directions are evaluated to identify the circumventing trajectory that advances toward the target most efficiently, as quantified by the penalty function $p(x^{(i)}, x^*) = \|x^{(i)}[:2] - x^*\|_2$.

C. Hospital Navigation Simulations

This section evaluates the proposed MCBF-QP controllers in a structured indoor environment resembling a hospital. The environment, adapted from Arena Rosnav [28], includes both convex and concave static furniture as well as dynamic

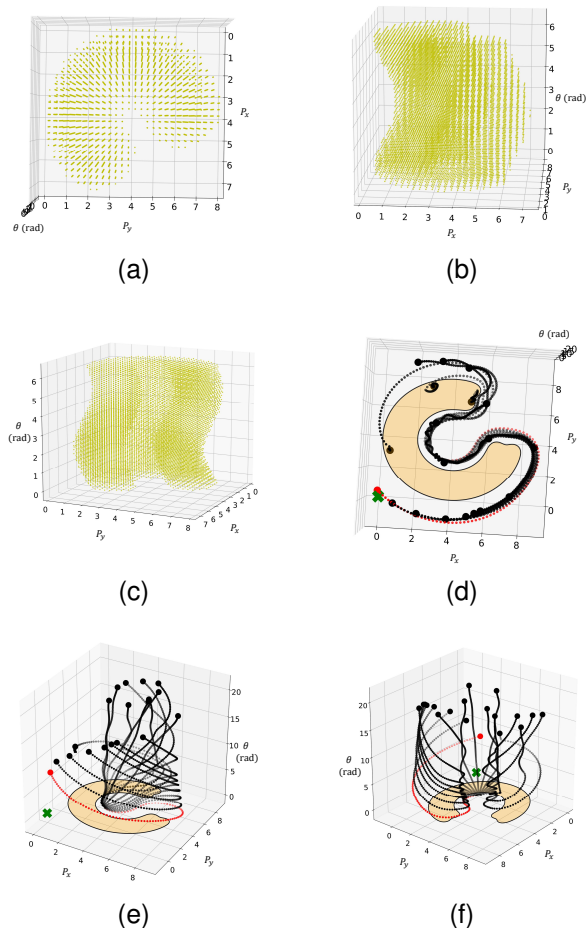


Fig. 10. Figures (a) - (c) show the top, side, and diagonal views of the unsafe regions defined by the augmented barrier function h_{aug} in Eq. (51). Figures (d) - (f) illustrate the same views with the geodesic approximation method applied: the selected circumventing trajectory is shown in red, leading efficiently toward the target location (green 'X') despite the non-Euclidean nature of the state space.

obstacles such as nurses and patients. Five representative scenarios with different initial and target locations are designed, as shown in 11a. These scenarios capture typical challenges encountered by delivery robots operating in crowded hospital settings. Scenario 1 tests navigation around a concave obstacle (front desk); Scenarios 2–3 (“mix” and “mix-reverse”) combine concave and convex obstacle-avoidance challenges; and Scenarios 4–5 involve only convex obstacles (benches). The resulting performance metrics are summarized in Fig. 12.

The resulting quantitative performance across all scenarios is evaluated, in both Gazebo and Python simulation environments, between the proposed Modulated CBF-QP controllers and existing reactive safe controllers, as summarized in Fig. 12. Specifically, R-MCBF-QP and onM-MCBF-QP are compared against normal Mod-DS (N-Mod-DS), reference Mod-DS (R-Mod-DS), on-manifold Mod-DS (onM-Mod-DS), and CBF-QP for fully actuated systems using the omnidirectional Ridgeback robot in Gazebo. For underactuated differential-drive systems, S-onM-MCBF-QP is compared with S-CBF-QP using the Fetch robot in Gazebo, while A-onM-MCBF-QP is

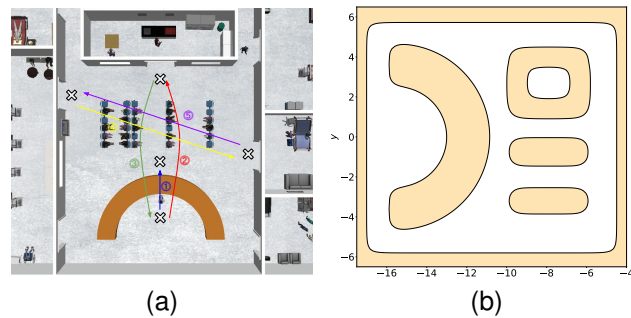
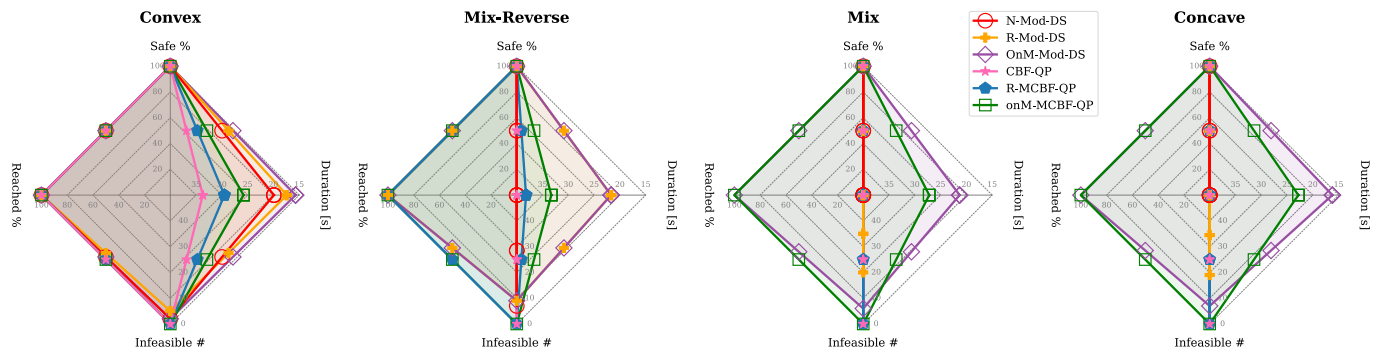


Fig. 11. Simulation environment and controller setup for robot comparison tests. Figure (a) presents the five test scenarios, while (b) depicts the robot’s perceived view of the hospital environment.

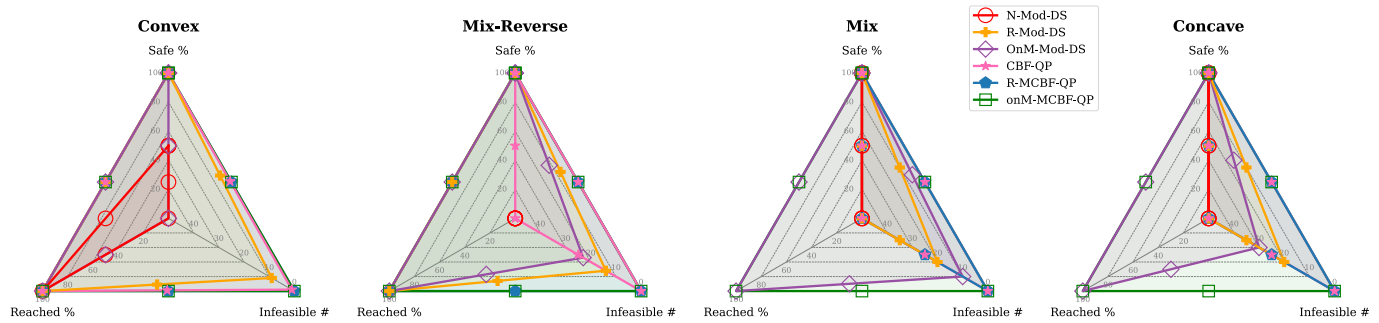
evaluated against A-CBF-QP within Python-based simulations. Since Mod-DS approaches are not applicable to underactuated systems, they are excluded from the corresponding comparisons. In Gazebo simulations, the robot repeats each navigation task ten times from a fixed initial pose to the target, while in Python simulations, it starts from the same position with ten different initial orientations. Performance is evaluated using four metrics: (i) average travel duration (s) from start to target, (ii) percentage of collision-free trajectories (Safe %), (iii) success rate of reaching the target (Reached %), and (iv) average number of infeasible QP instances per trajectory. All results are summarized in Fig. 12, where the metrics are normalized between the center and outermost layer of each spider plot, with tick marks indicating the corresponding value ranges. A larger radial extent of a metric indicates better performance in that aspect.

From the collected results, several conclusions emerge. In fully actuated systems (12a, 12b), Mod-DS methods (N-Mod-DS, R-Mod-DS, onM-Mod-DS) generally achieve shorter travel durations than CBF-QP-based controllers (CBF-QP, R-MCBF-QP, onM-MCBF-QP), consistent with Table II showing higher near-obstacle velocities. Both approaches ensure safety by decelerating along obstacle normals, but Mod-DS further accelerates tangentially, improving efficiency while increasing infeasibility risks in dense, multi-obstacle settings. When obstacles are closely spaced, Mod-DS exhibits reduced safety performance, as indicated by Safe % values of 50% and 0% for N-Mod-DS in the dynamic convex and mix-reverse environments, respectively. In contrast, CBF-QP, proven theoretically equivalent to N-Mod-DS in single-obstacle avoidance (Theorem V.2), remains robust under these conditions. The proposed R-MCBF-QP and onM-MCBF-QP methods overcome these limitations by maintaining the 100 Safe %, equivalent to that of CBF-QP, while substantially reducing infeasibility compared to Mod-DS approaches. Furthermore, R-MCBF-QP achieves a 100 % reaching rate in the mix-reverse scenario, and onM-MCBF-QP attains 100 % reachability across all tested environments. In contrast, CBF-QP fails to complete any tasks under mix, mix-reverse, or concave scenarios.

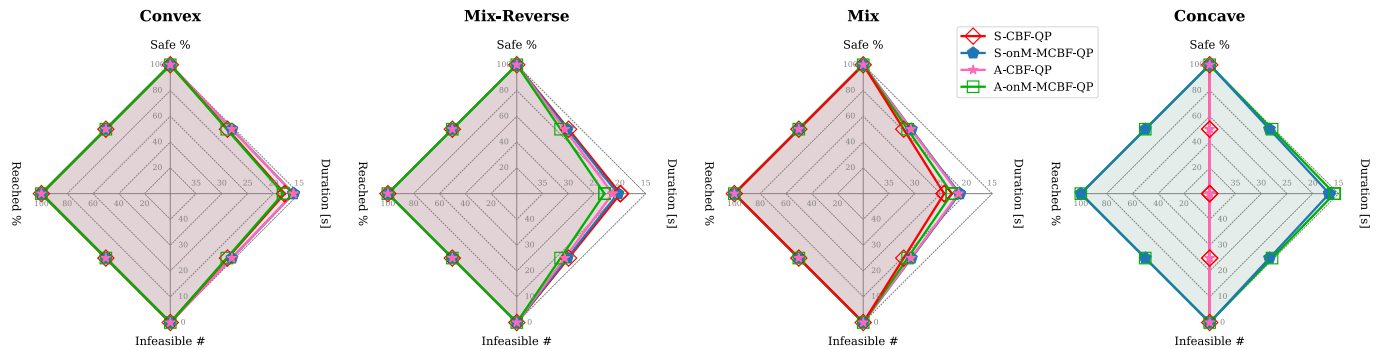
In underactuated differential-drive systems (12c, 12d), both conventional CBF-QP methods (S-CBF-QP and A-CBF-QP)



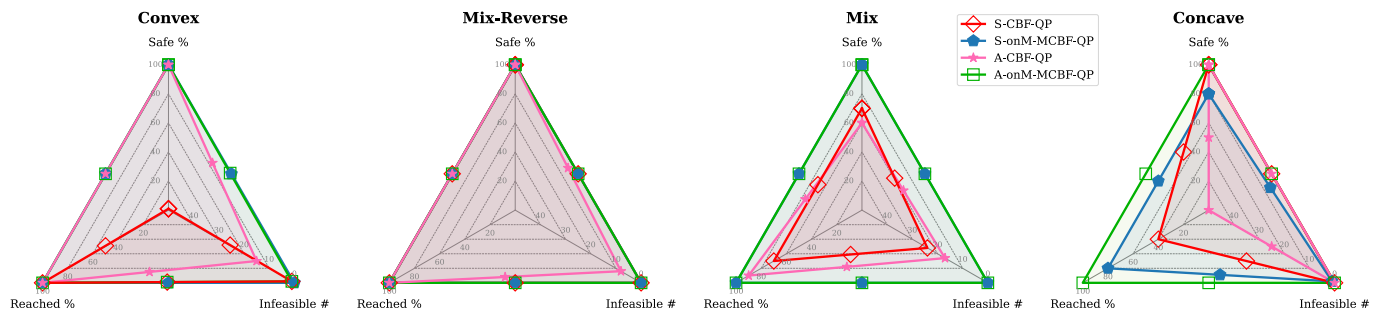
(a) Fully Actuated Systems in Static Environment



(b) Fully Actuated Systems in Dynamic Environment



(c) Under-Actuated Systems in Static Environment



(d) Under-Actuated Systems in Dynamic Environment

Fig. 12. Spider plot summarizing controller performance in hospital navigation at 20 Hz. Metrics include average travel duration, Safe %, Reached %, and average number of infeasible QP instances per trajectory. Values are normalized between the center and outermost layer, where a larger radial extent denotes better performance.

and the proposed modulated variants (S-onM-MCBF-QP and A-onM-MCBF-QP) provide strong safety guarantees, with collisions occurring only in rare cases of QP infeasibility

in dynamic environments. However, the proposed MCBF-QP controllers significantly improve goal-reaching performance in concave environments. Furthermore, in most scenarios, they

achieve shorter travel durations, as the tangential velocity component inherited from onM-Mod-DS guides the robot along more efficient paths.

Overall, experiments in simulated hospital environments demonstrate that the proposed Modulated CBF-QP methods outperform both Mod-DS and standard CBF-QP baselines across fully actuated and underactuated control-affine systems.

D. Real World Experiments

In addition to simulations, the proposed S-onM-MCBF-QP and A-onM-MCBF-QP methods are compared to S-CBF-QP and A-CBF-QP in real-life experiments using Fetch given nominal controller in Eq. (52). In the first experiment, Fetch is challenged to reach the goal position on the other side of the room despite active attempts from a walking human to block its path. In the second experiment, the robot is tasked to navigate out of a C-shaped cluster region towards the target. These two experiments are repeated five times with different robot initial poses in static scenarios and different human walking trajectories in dynamic scenarios. Lastly, we validated our proposed method in a real-life social navigation experiment using the robot Fetch to avoid a 3-person cluster while reaching the target, as presented in 1a. In all hardware experiments, a Vicon motion tracking system was used to capture real-time positions and velocities of both humans and the robot.

The performances of the onM-MCBF-QPs and CBF-QPs in hardware experiments are summarized in Table III, where “Safe %” denotes the percentage of collision-free trajectories, “Reached %” indicates the probability of the robot reaching the target, and “Duration (s)” specifies the time (in seconds) required for the robot to travel from the initial to the target locations. The results demonstrate that CBF-induced local minima will deteriorate robot task completion performance, while the introduction of onM-Mod-based constraints into the same QP problem can sufficiently eliminate those local minima. In 2D navigation tasks using Fetch, though both A-onM-MCBF-QP and S-onM-MCBF-QP drastically improve robot task completion performance, S-onM-MCBF-QP using the shifted unicycle model outperforms A-onM-MCBF-QP using the standard unicycle model in terms of path efficiency and task completion rate. The reason for that is the unsafe region defined by A-CBF $h_{\text{aug}}(x, x_o)$ (51), as shown in 10c, is not the same as the actual obstacle region, causing the geodesic approximation strategy to output sometimes non-optimal choices of tangent vectors $\phi(x, x_o)$ for the robot to track. Additionally, finding an appropriate step size β and horizon N to use during geodesic approximation is more challenging for A-MCBF-QP that searches for $\phi(x, x_o)$ in 3D non-Euclidean state spaces, compared with S-MCBF-QP that looks for $\phi(p_x, p_y, x_o)$ instead in 2D Euclidean spaces. Nevertheless, A-onM-MCBF-QP offers the merit of generalizability, as it can, in principle, be applied to any control-affine robot model.

VIII. DISCUSSION AND FUTURE DIRECTIONS

By quantitatively, qualitatively, and analytically comparing optimization-based CBF-QP, closed-form Mod-DS methods, and the proposed Modulated CBF-QP approach in both static

TABLE III
PERFORMANCES OF PROPOSED ONMANIFOLD-MODULATED CBF-QP METHODS IN COMPARISON TO CBF-QP FORMULATIONS IN REAL-LIFE EXPERIMENTS USING FETCH AT 20HZ. “NA” DENOTES “NOT APPLICABLE,” INDICATING THAT THE DURATION CANNOT BE RECORDED BECAUSE THE ROBOT NEVER REACHES THE TARGET.

Scenario	Methods	Safe %	Reached %	Duration (s)
convex dynamic	S-CBF	100	0	NA
	S-onM-MCBF	100	100	12.4
	A-CBF	100	0	NA
	A-onM-MCBF	100	100	14.3
static concave	S-CBF	100	0	NA
	S-onM-MCBF	100	100	14.9
	A-CBF	100	0	NA
	A-onM-MCBF	100	80	30.7

and dynamic obstacle environments, the following conclusions can be drawn for safe navigation using single-integrator and differential drive systems:

- 1) In static and sparsely populated dynamic environments, Mod-DS approaches, including reference Mod-DS and on-manifold Mod-DS, handle concave obstacles more effectively than CBF-QP by inducing fewer undesirable equilibria on the boundary set $\partial\mathcal{C}$. Yet, their applicability is limited to fully actuated systems.
- 2) In densely crowded dynamic environments, CBF-QP provides stronger safety guarantees than Mod-DS. However, convergence to target locations cannot be guaranteed in the presence of concave obstacles.
- 3) Compared with Mod-DSs and CBF-QPs, the proposed Modulated CBF-QP achieves superior performance by combining the strengths of Mod-DS in eliminating undesirable local minima with the safety robustness and generalizability of CBF-QP.

In this work, the proposed Modulated CBF-QP methods are validated using omni-directional and differential-drive robot dynamics. Beyond locomotion, however, robot manipulation tasks are also susceptible to performance degradation due to local minima arising from concave joint spaces. Extending on-manifold Modulated CBF-QP to achieve local-minimum-free manipulation is an interesting direction to explore. In addition, the effectiveness of tangent-direction selection via the geodesic approximation strategy depends on appropriate user tuning of the parameters β and N . Automating this tuning process through analytic or learning-based methods, particularly to enable Modulated CBF-QP to maintain local-minimum-free navigation in the presence of continuously deforming dynamic obstacles, represents a promising avenue for future research. Finally, the introduction of additional modulation constraints in CBF-QPs inevitably reduces the instantaneous feasible set of on-manifold MCBF-QP. Since these constraints are enforced within a one-step, myopic optimization framework, the obstacle exit strategy $\phi(x, x_o)$ selected at the current state does not, in general, guarantee forward feasibility of the resulting closed-loop system. A principled approach to addressing this limitation is to incorporate analogous tangent-hyperplane guidance into receding-horizon frameworks, which constitutes another important avenue for future work.

REFERENCES

- [1] P. A. Lasota, T. Fong, and J. A. Shah, "A survey of methods for safe human-robot interaction," *Foundations and Trends® in Robotics*, vol. 5, no. 4, pp. 261–349, 2017.
- [2] A. D. Ames, S. Coogan, M. Egerstedt, G. Notomista, K. Sreenath, and P. Tabuada, "Control barrier functions: Theory and applications," in *2019 18th European control conference (ECC)*. IEEE, 2019, pp. 3420–3431.
- [3] J. Zeng, B. Zhang, and K. Sreenath, "Safety-critical model predictive control with discrete-time control barrier function," in *2021 American Control Conference (ACC)*. IEEE, 2021, pp. 3882–3889.
- [4] Y. Emam, P. Glotfelter, S. Wilson, G. Notomista, and M. Egerstedt, "Data-driven robust barrier functions for safe, long-term operation," *IEEE Transactions on Robotics*, vol. 38, no. 3, pp. 1671–1685, 2022.
- [5] A. Singletary, S. Kolathaya, and A. D. Ames, "Safety-critical kinematic control of robotic systems," *IEEE Control Systems Letters*, vol. 6, pp. 139–144, 2022.
- [6] M. Saveriano and D. Lee, "Learning barrier functions for constrained motion planning with dynamical systems," in *2019 IEEE/RSJ International Conference on Intelligent Robots and Systems (IROS)*, 2019, pp. 112–119.
- [7] I. Jang and H. J. Kim, "Safe control for navigation in cluttered space using multiple lyapunov-based control barrier functions," *IEEE Robotics and Automation Letters*, vol. 9, no. 3, pp. 2056–2063, 2024.
- [8] J. Borenstein and Y. Koren, "Real-time obstacle avoidance for fast mobile robots," *IEEE Transactions on systems, Man, and Cybernetics*, vol. 19, no. 5, pp. 1179–1187, 1989.
- [9] E. Rimon and D. Koditschek, "Exact robot navigation using artificial potential functions," *IEEE Transactions on Robotics and Automation*, vol. 8, no. 5, pp. 501–518, 1992.
- [10] H. J. S. Feder and J.-J. Slotine, "Real-time path planning using harmonic potentials in dynamic environments," in *Proceedings of International Conference on Robotics and Automation*, vol. 1. IEEE, 1997, pp. 874–881.
- [11] S. M. Khansari-Zadeh and A. Billard, "A dynamical system approach to realtime obstacle avoidance," *Autonomous Robots*, vol. 32, pp. 433–454, 2012.
- [12] M. Saveriano and D. Lee, "Distance based dynamical system modulation for reactive avoidance of moving obstacles," in *2014 IEEE International Conference on Robotics and Automation (ICRA)*, 2014, pp. 5618–5623.
- [13] L. Huber, A. Billard, and J.-J. Slotine, "Avoidance of convex and concave obstacles with convergence ensured through contraction," *IEEE Robotics and Automation Letters*, vol. 4, no. 2, pp. 1462–1469, 2019.
- [14] A. Billard, S. Mirrazavi, and N. Figueroa, *Learning for Adaptive and Reactive Robot Control: A Dynamical Systems Approach*. MIT Press, 2022.
- [15] A. Dahlin and Y. Karayiannidis, "Creating star worlds: Reshaping the robot workspace for online motion planning," *IEEE Transactions on Robotics*, vol. 39, no. 5, pp. 3655–3670, 2023.
- [16] M. F. Reis, A. P. Aguiar, and P. Tabuada, "Control barrier function-based quadratic programs introduce undesirable asymptotically stable equilibria," *IEEE Control Systems Letters*, vol. 5, no. 2, pp. 731–736, 2021.
- [17] A. Singletary, K. Klingebiel, J. Bourne, A. Browning, P. Tokumaru, and A. Ames, "Comparative analysis of control barrier functions and artificial potential fields for obstacle avoidance," in *2021 IEEE/RSJ International Conference on Intelligent Robots and Systems (IROS)*. IEEE, 2021, pp. 8129–8136.
- [18] M. Spong, S. Hutchinson, and M. Vidyasagar, "Robot modeling and control," *IEEE Control Systems*, vol. 26, no. 6, pp. 113–115, Dec. 2006.
- [19] C. K. Fourie, N. Figueroa, and J. A. Shah, "On-manifold strategies for reactive dynamical system modulation with nonconvex obstacles," *IEEE Transactions on Robotics*, vol. 40, pp. 2390–2409, 2024.
- [20] M. Eisenberg and R. Guy, "A proof of the hairy ball theorem," *The American Mathematical Monthly*, vol. 86, no. 7, pp. 571–574, 1979.
- [21] Z. Li, "Comparison between safety methods control barrier function vs. reachability analysis," *arXiv preprint arXiv:2106.13176*, 2021.
- [22] Y. Lin, J. McPhee, and N. L. Azad, "Comparison of deep reinforcement learning and model predictive control for adaptive cruise control," *IEEE Transactions on Intelligent Vehicles*, vol. 6, no. 2, pp. 221–231, 2021.
- [23] D. E. Koditschek and E. Rimon, "Robot navigation functions on manifolds with boundary," *Advances in Applied Mathematics*, vol. 11, no. 4, pp. 412–442, 1990.
- [24] S. Sakaguchi, "Star shaped coincidence sets in the obstacle problem," *Annali della Scuola Normale Superiore di Pisa - Classe di Scienze*, vol. 11, no. 1, pp. 123–128, 1984.
- [25] H. J. Choi and N. Figueroa, "Towards feasible dynamic grasping: Leveraging gaussian process distance field, se(3) equivariance, and riemannian mixture models," in *IEEE International Conference on Robotics and Automation (ICRA)*, 2024, pp. 6455–6461.
- [26] Y. Zhou, S. Booth, N. Figueroa, and J. Shah, "Rocus: Robot controller understanding via sampling," in *Conference on Robot Learning*. PMLR, 2022, pp. 850–860.
- [27] G. Notomista and M. Saveriano, "Safety of dynamical systems with multiple non-convex unsafe sets using control barrier functions," *IEEE Control Systems Letters*, vol. 6, pp. 1136–1141, 2021.
- [28] Arena-Rosnav, "Repository name," <https://github.com/Arena-Rosnav>, 2025, gitHub repository.
- [29] L. Huber, J.-J. Slotine, and A. Billard, "Avoiding dense and dynamic obstacles in enclosed spaces: Application to moving in crowds," *IEEE Transactions on Robotics*, vol. 38, no. 5, pp. 3113–3132, 2022.

APPENDIX

A. Variable Dictionary

TABLE IV
KEY VARIABLES IN THIS PAPER.

Variable	Description
x	Robot state vector
x^*	Target position for trajectory planning
p_x	Robot position along the x -axis
p_y	Robot position along the y -axis
θ	Robot heading/orientation
x_o	Obstacle state vector
u	Robot control input vector
v	Unicycle linear velocity
ω	Unicycle angular velocity
u_{nom}	Nominal control input
$\alpha(\cdot)$	Class- \mathcal{K} function
$h(\cdot)$	Control barrier function (CBF)
$h_{\text{aug}}(\cdot)$	Augmented Control Barrier Function (A-CBF)
$H(\cdot)$	Hyperplane tangent to obstacle surface
$E(\cdot)$	Orthonormal obstacle-based frame
$E_r(\cdot)$	Non-orthonormal reference Mod-DS frame
$n(\cdot)$	Unit vector normal to the obstacle boundary
$r(\cdot)$	Reference vector defined in Eq. (23)
$e_i(\cdot)$	Orthonormal basis vectors spanning the tangent hyperplane $H(\cdot)$
λ	Normal direction scaling coefficient in Mod-DS
λ_e	Tangent direction scaling coefficient in Mod-DS
ρ	Slack variables in Eq. (34)
β	Step size parameter in geodesic approximation
N	Horizon size in geodesic approximation
$p(x, x^*)$	User-defined penalty function, typically chosen as the distance from x to the target x^*
$\phi(\cdot)$	Tangent-hyperplane guidance vector estimated using geodesic approximation
γ	User-defined positive real number in Eq. (46)

B. Metrics for Collision Avoidance Evaluation

TABLE V
BEHAVIOR METRICS FOR COLLISION AVOIDANCE COMPARISON (ADAPTED FROM [26]).

Metric	Equation
Trajectory Length	$l = \int_{\tau} 1 ds$
Average Jerk	$\bar{j} = \frac{1}{l} \int_{\tau} \ \ddot{x}\ _2 ds$
Straight-Line Deviation	$\eta = \frac{1}{l} \int_{\tau} \ x - \text{proj}_{x^* - x_{\text{ini}}}(x)\ _2 ds$
Obstacle Clearance	$d_{\text{obs}} = \frac{1}{l} \int_{\tau} \min_{x' \in -\mathcal{C}} \ x - x'\ _2 ds$
Near-Obstacle Velocity	$v_{\text{near}} = \frac{\int_{\tau} \ \dot{x}\ / \min_{x' \in -\mathcal{C}} \ x - x'\ _2 ds}{\int_{\tau} 1 / \min_{x' \in -\mathcal{C}} \ x - x'\ _2 ds}$

C. Constrained Mod-DS in Fully-Actuated Systems

In Section IV, Mod-DS's strength in navigating around a larger variety of obstacles with fewer undesirable local minima is demonstrated, which makes it a more suitable option for robots with fully actuated systems. However, some may argue that all Mod-DS approaches have limitations in handling input constraints. For closed-form methods in general, implementing velocity constraints poses challenges as modifications to the modulated velocity might compromise the agent's guaranteed impenetrability. Here in this section, by posing Mod-DS's input constraining process as an independent convex optimization problem and proving mathematically that such optimization problem either has simple closed-form solutions or can be solved sufficiently fast, we argue that Mod-DS's constraints enforcement ability in fully-actuated systems is equivalent to that of CBF-QP. In robot applications, inputs constraints typically can be categorized into 2 types: speed constraints $\|\dot{x}\|_2 = \|u\|_2 \leq u_{\text{ub}}$, and velocity or box constraints $U_{\text{lb}} \leq u \leq U_{\text{ub}}$, where $u_{\text{ub}} \in \mathbb{R}$ and $U_{\text{lb}}, U_{\text{ub}} \in \mathbb{R}^d$. Following, one optimization problem is constructed for each constraint type. We again abused notation here and set $n = n(x, x_o)$, which is defined in Eq. (21).

D. Speed-Constraining Mod-DS

When the unconstrained output from Mod-DS $u_{\text{unc}} = \dot{x}_{\text{unc}}$ exceeds the speed limit, solving the following Quadratically Constrained Linear Programming (QCLP) problem finds the constrained output u_c that is most similar to u_{unc} and ensures safety defined in Eq. (55) while satisfying speed input constraint u_{ub} in Eq. (54). In both speed-constraining and velocity-constraining Mod-DS, robot safety is ensured by restricting the robot's velocity moving towards the obstacle, i.e. the projection of u_c onto vector $n(x, x_o)$, to be no larger than that of u_{unc} .

$$u_c = \arg \max_u \langle u_{\text{unc}}, u \rangle \quad (53)$$

$$\|u\|_2 \leq u_{\text{ub}} \quad (54)$$

$$\langle n, u \rangle \geq \min(\langle n, \bar{x}_o \rangle, \langle n, u_{\text{unc}} \rangle) \quad (55)$$

In speed-constraining Mod-DS, we make the design choice to measure similarity between the constrained and unconstrained Mod-DS outputs using dot products between the two vectors

so that the QP has simple closed-form solutions. Using dot products as cost functions is reasonable because $\langle u_{\text{unc}}, u \rangle = \|u_{\text{unc}}\|_2 \|u\|_2 \cos \theta_d$, where $\theta_d \in [0, \pi]$ is the angle difference between the two vectors. $\|u_{\text{unc}}\|_2$ is fixed because u_{unc} is a constant vector input into the QP. When $\|u\|_2$ is also fixed, the dot product between u_{unc} and u is inversely correlated to θ_d . In other words, the larger the dot product is, the more similar u is to u_{unc} orientation-wise. We know the magnitude of the optimal solution of the QP u_c must be fixed to $\|u_c\|_2 = u_{\text{ub}}$, because the above optimization problem would only be called to modify u_{unc} when $\|u_{\text{unc}}\|_2 > u_{\text{ub}}$. Therefore, the optimization problem can be reformulated as the following. Note that $\langle a, b \rangle = a^\top b$ when $a, b \in \mathbb{R}^d$ and $\|u\|_2^2 = u^\top u$.

$$\begin{aligned} u_c &= \arg \max_u u_{\text{unc}}^\top u & (56) \\ u^\top u &= (u_{\text{ub}})^2 \\ n^\top u &\geq \min(n^\top \bar{x}_o, n^\top u_{\text{unc}}) \end{aligned}$$

Denote $v_n = \min(n^\top \bar{x}_o, n^\top u_{\text{unc}})$. Solving for the explicit solutions of the above convex optimization problem using Karush–Kuhn–Tucker (KKT) conditions, a simple explicit solution is found as in Eq. (57), where $v_e = \sqrt{\|u_{\text{unc}}\|_2^2 - \|n^\top u_{\text{unc}}\|_2^2} = \|H^\top u_{\text{unc}}\|_2$ is the projection of u_{unc} onto the tangent hyperplane $H = H(x, x_o)$ defined in Eq. (19).

$$\begin{cases} \frac{u_{\text{ub}}}{\|u_{\text{unc}}\|_2} u_{\text{unc}} & \text{if } \frac{u_{\text{ub}}}{\|u_{\text{unc}}\|_2} n^\top u_{\text{unc}} \geq v_n \\ v_n n + \frac{\sqrt{(u_{\text{ub}})^2 - (v_n)^2}}{v_e} (u_{\text{unc}} - u_{\text{unc}}^\top n n) & \text{otherwise} \end{cases} \quad (57)$$

The difference between the proposed method with the strategy in [29] is that ours considers the unconstrained Mod-DS outputs $n^\top u_{\text{unc}}$ when determining whether the robot is safe, which improves the smoothness of the trajectories generated by the constrained outputs and maximumly preserves the Mod-DS characteristics (see Fig. 13).

E. Velocity-Constraining Mod-DS

Similarly, solving optimization problem in Eq. (58) offers solutions to enforcing velocity constraints $U_{\text{lb}} \leq u \leq U_{\text{ub}}$ for Mod-DS in fully-actuated systems while guaranteeing safety.

$$\begin{aligned} u_c &= \arg \min_u \|u - u_{\text{unc}}\|_2^2 & (58) \\ U_{\text{lb}} &\leq u \leq U_{\text{ub}} \\ n^\top u &\geq \min(n^\top \bar{x}_o, n^\top u_{\text{unc}}) \end{aligned}$$

Unlike the speed-constraining Mod-DS, the QP problem for enforcing velocity constraints no longer has a straightforward explicit solution, because the complexity of the explicit solution derived from KKT conditions grows exponentially with the number of inequality constraints in the problem. Note that both speed-constraining and velocity-constraining Mod-DS methods proposed here remain valid for high dimensional state-spaces when $d > 3$.

F. Theoretical Guarantees

Both speed and velocity constraining Mod-DS preserve the *impenetrability* guarantees of the original Mod-DS, under the

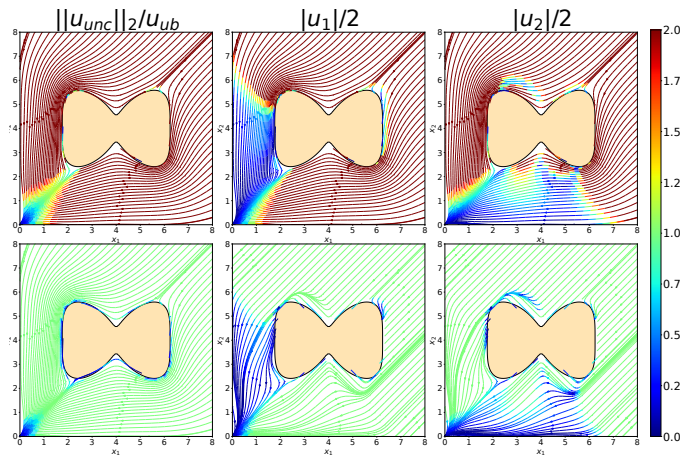


Fig. 13. Unconstrained reference Mod-DS (first row) vs. speed-constrained (second row, left) and velocity-constrained reference Mod-DS with $U_{\text{ub}} = -U_{\text{lb}} = [2, 2]^\top$ (second row, middle and right). The color codes for images in the left, middle, and right columns respectively represent $\frac{\|u_{\text{unc}}\|_2}{u_{\text{ub}}}$, $\frac{|u_1|}{2}$, and $\frac{|u_2|}{2}$, given that $u = [u_1, u_2]^\top$.

assumption that the speed that the obstacle travels towards the agent is no more than the speed limit. We showcase stream plots in Fig. 13 to demonstrate performances of speed-constraining and velocity-constraining Mod-DS compared to unconstrained Mod-DS.

Theorem A.1. Consider an obstacle whose boundary is defined as $h(x, x_o) = 0$. Any trajectory $x(t)$, $t \in [0, \infty)$ starting outside the obstacle boundary, i.e., $h(x(0), x_o(0)) \geq 0$, evolving according to Eq. (16) and being constrained by the Speed-Constraining and Velocity-Constraining approaches Mod-DS presented in Appendix D and E, will never penetrate the obstacle boundary, i.e., $h(x(t), x_o(t)) \geq 0$, $\forall t \in [0, \infty)$.

Proof: In [11], [13], and [19], the unconstrained outputs u_{unc} from respectively normal, reference and on-manifold Mod-DS approaches are proven to achieve obstacle impenetrability in terms of the von Neuman boundary condition, listed in Eq. (59).

$$n(x, x_o)^\top u_{\text{unc}} = 0 \quad \forall x \in \partial \mathcal{C}_o \quad (59)$$

Given safe controller u_{unc} in Eq. (59), we want to show that the constrained solutions u_c of the QPs in (56) and (58) also satisfies the set invariance condition of impenetrability. In other words,

$$n(x, x_o)^\top u_c \geq 0 \quad \forall x \in \partial \mathcal{C}_o \quad (60)$$

Since any solutions u_c from QPs in (56) and (58) must satisfy the safety constraints in (55), $n(x, x_o)^\top u_c \geq n(x, x_o)^\top u_{\text{unc}}$ must be true for all state x . This implies that $n(x, x_o)^\top u_c \geq 0$ if $n(x, x_o)^\top u_{\text{unc}} = 0$. Therefore, the statement in (60) always holds. ■